



OPEN ACCESS

ORIGINAL ARTICLE

Signalling via the osteopontin and high mobility group box-1 axis drives the fibrogenic response to liver injury

Elena Arriazu,¹ Xiaodong Ge,^{1,2} Tung-Ming Leung,¹ Fernando Magdaleno,^{1,2} Aritz Lopategi,¹ Yongke Lu,¹ Naoto Kitamura,¹ Raquel Urtasun,¹ Neil Theise,³ Daniel J Antoine,⁴ Natalia Nieto^{1,2}

► Additional material is published online only. To view please visit the journal online (<http://dx.doi.org/10.1136/gutjnl-2015-310752>).

¹Division of Liver Diseases, Department of Medicine, Icahn School of Medicine at Mount Sinai, New York, New York, USA

²Department of Pathology, University of Illinois at Chicago, Chicago, Illinois, USA

³Division of Digestive Diseases, Mount Sinai Beth Israel Medical Center, New York, New York, USA

⁴Medical Research Council Centre for Drug Safety Science, Molecular and Clinical Pharmacology, University of Liverpool, Liverpool, UK

Correspondence to

Dr Natalia Nieto, Department of Pathology, University of Illinois at Chicago, 840 S. Wood St., Suite 130 CSN, MC 847, Chicago IL 60612, USA; nnieto@uic.edu

EA and XG contributed equally.

Received 21 September 2015

Revised 17 December 2015

Accepted 28 December 2015

Published Online First

27 January 2016

ABSTRACT

Objective Liver fibrosis is associated with significant collagen-I deposition largely produced by activated hepatic stellate cells (HSCs); yet, the link between hepatocyte damage and the HSC profibrogenic response remains unclear. Here we show significant induction of osteopontin (OPN) and high-mobility group box-1 (HMGB1) in liver fibrosis. Since OPN was identified as upstream of HMGB1, we hypothesised that OPN could participate in the pathogenesis of liver fibrosis by increasing HMGB1 to upregulate collagen-I expression.

Design and results Patients with long-term hepatitis C virus (HCV) progressing in disease stage displayed enhanced hepatic OPN and HMGB1 immunostaining, which correlated with fibrosis stage, whereas it remained similar in non-progressors. Hepatocyte cytoplasmic OPN and HMGB1 expression was significant while loss of nuclear HMGB1 occurred in patients with HCV-induced fibrosis compared with healthy explants. Well-established liver fibrosis along with marked induction of HMGB1 occurred in CCl₄-injected *Opn*^{Hep} transgenic yet it was less in wild type and almost absent in *Opn*^{-/-} mice. *Hmgb1* ablation in hepatocytes (*Hmgb1*^{ΔHep}) protected mice from CCl₄-induced liver fibrosis. Coculture with hepatocytes that secrete OPN plus HMGB1 and challenge with recombinant OPN (rOPN) or HMGB1 (rHMGB1) enhanced collagen-I expression in HSCs, which was blunted by neutralising antibodies (Abs) and by *Opn* or *Hmgb1* ablation. rOPN induced acetylation of HMGB1 in HSCs due to increased NADPH oxidase activity and the associated decrease in histone deacetylases 1/2 leading to upregulation of collagen-I. Last, rHMGB1 signalled via receptor for advanced glycation end-products and activated the PI3K–pAkt1/2/3 pathway to upregulate collagen-I.

Conclusions During liver fibrosis, the increase in OPN induces HMGB1, which acts as a downstream alarmin driving collagen-I synthesis in HSCs.

INTRODUCTION

Fibrogenesis encompasses qualitative and quantitative changes in the extracellular matrix (ECM) deposits with a significant buildup of collagen-I fibers, largely produced by activated hepatic stellate cells (HSCs), which extensively distort the normal hepatic architecture. Failure to degrade the

Significance of this study

What is already known on this subject?

- Osteopontin (OPN) and high-mobility group box-1 (HMGB1) are expressed in human and mouse liver.
- We previously demonstrated the mechanisms driving the increase in OPN in liver fibrosis; yet, whether OPN could increase HMGB1 has not been established.
- If besides the profibrogenic mechanisms previously identified by us, OPN targets HMGB1 to activate extracellular matrix deposition by hepatic stellate cells (HSCs) remained unknown.

What are the new findings?

- OPN and HMGB1 expression correlate with fibrosis stage in humans and mice.
- Using in vivo and in vitro loss or gain of function approaches, we demonstrate that OPN is upstream of HMGB1.
- Extracellular OPN promotes the acetylation of intracellular HMGB1 in HSCs due to increased NADPH oxidase activity and the associated decrease in histone deacetylases 1/2 leading to upregulation of collagen-I.
- Extracellular HMGB1 signals HSCs via the receptor for advanced glycation end-products activating the PI3K–pAkt1/2/3 pathway to increase collagen-I deposition.

How might it impact on clinical practice in the foreseeable future?

- Identification of key mediators along with better understanding of the signalling pathways they trigger to promote fibrosis is critical to prevent disease progression and design new therapies. This study reinforces the role of HMGB1, a hepatic sterile damage-associated molecular pattern, in the progression of liver fibrosis. The role of OPN and HMGB1 on collagen-I production by HSCs reveals novel signalling mechanisms that could be targeted for therapeutic benefit.



CrossMark

To cite: Arriazu E, Ge X, Leung T-M, et al. *Gut* 2017;**66**:1123–1137.

progressive increase in scar tissue is a major reason why fibrosis evolves into cirrhosis and hepatocellular carcinoma. To date, extensive research has focused on identifying the key factors involved in the pathogenesis of liver fibrosis; yet, the precise link between injured hepatocytes, HSCs and the fibrogenic response still remains poorly defined.

We have previously shown that osteopontin (OPN), a matrix-bound protein sensitive to oxidant stress and highly induced upon liver damage, plays a central role in the pathogenesis of liver fibrosis by contributing to ECM deposition.^{1–3} Mechanistic studies revealed first that OPN upregulates collagen-I production by HSCs via integrin $\alpha_v\beta_3$ engagement and activation of the PI3K–pAkt1/2/3–NF κ B signalling pathway;³ and second, that OPN drives ductular reaction contributing to periportal scarring by increasing transforming growth factor (TGF) β production in biliary epithelial cells;¹ yet, additional mediators downstream of OPN, perhaps with profibrogenic potential, could participate increasing pathological collagen-I deposition by HSCs.

High-mobility group box-1 (HMGB1) is a nuclear non-histone chromosomal protein that binds the DNA minor groove and is involved in DNA replication, repair and energy homeostasis.⁴ Initially, it was believed that HMGB1 acted primarily as an architectural protein. However, upon cellular injury and post-translational modifications (PTMs), HMGB1 undergoes translocation from the nucleus to the cytoplasm and is secreted via the lysosomal pathway in most cells.⁵ HMGB1 signals via the receptor for advanced glycation end-products (RAGE), toll-like receptors (TLRs)-2/4/9, Mac-1, syndecan-1, phosphacan protein-tyrosine phosphatase- ζ/β and CD24.⁶

Recent work from our laboratory has demonstrated that HMGB1 has noxious effects in the hepatic environment in the setting of alcoholic liver disease.⁷ When released from injured or necrotic cells due to loss of membrane integrity⁸ or when secreted by hepatocytes in response to ethanol,⁷ HMGB1 can trigger harmful responses. Thus, HMGB1 is now considered a member of the family of damage-associated molecular patterns (DAMPs) that communicate injury to neighbouring cells.

Although this alarmin increases in plasma and liver from alcoholic and fibrotic patients,^{7,9} it is unknown whether it plays a direct role in liver fibrosis. Our preliminary in vivo observations suggested that OPN is upstream of HMGB1 in hepatocytes and HSCs. To date, whether OPN by increasing HMGB1 in a paracrine and/or in an autocrine fashion could regulate collagen-I deposition in HSCs has not been demonstrated. Thus, we hypothesised that OPN by upregulating HMGB1 could participate in the pathogenesis of liver fibrosis driving scarring. Using in vivo and in vitro loss-of-function or gain-of-function approaches we focused on dissecting how the OPN and HMGB1 axis in hepatocytes and HSCs regulates the HSC profibrogenic behaviour. Overall, the data show that intracellular OPN increases HMGB1 expression and extracellular OPN induces acetylation of HMGB1 in HSCs due to increased NADPH oxidase (NOX) activity and the associated decrease in histone deacetylases (HDACs) 1/2 leading to upregulation of collagen-I. Thus, OPN has autocrine and paracrine effects in HSCs. Moreover, extracellular HMGB1 upregulates collagen-I expression in HSCs paracrinely due to RAGE activation of the PI3K–pAkt1/2/3 signalling pathway; thus, contributing to the pathogenesis of liver fibrosis.

MATERIALS AND METHODS

Mice

C57BL/6J wild-type (WT) and *Opn*^{−/−} (B6.Cg-*Spp1*^{tm1Blh}/J) mice were obtained from the Jackson Laboratory (Bar Harbor,

Maine, USA). *Opn*^{+/-} mice were intercrossed and littermates were used in all experiments. The *Opn* transgenic mice overexpressing OPN in hepatocytes (*Opn*^{Hep} Tg) under the serum amyloid-P component promoter were donated by Dr Mochida (Saitama Medical University, Saitama, Japan).¹⁰ These mice were crossbred for 10 generations with the same strain and stock number of C57BL/6J WT listed above. The *Hmgb1*^{fl/fl} mice were donated by Dr Billiar (University of Pittsburgh, Pittsburgh, Pennsylvania, USA). In these mice, the *Hmgb1*^{loxP} allele was created by inserting *loxP* sites within introns 1 and 2 flanking exon 2 of *Hmgb1*.¹¹ The *Hmgb1*^{fl/fl} mice were bred with *Alb.Cre* mice (the Jackson Laboratory) to generate hepatocyte-specific *Hmgb1*^{fl/fl}*Alb.Cre* mice (abbreviated as *Hmgb1*^{ΔHep}). All animals received humane care according to the criteria outlined in the 'Guide for the Care and Use of Laboratory Animals' prepared by the National Academy of Sciences and published by the National Institutes of Health.

Statistical analysis

Data were analysed by a two-factor analysis of variance. All in vitro experiments were performed in triplicate at least four times. A representative blot is shown in all figures. Eight mice per group were used in all the in vivo experiments, which were repeated twice.

RESULTS

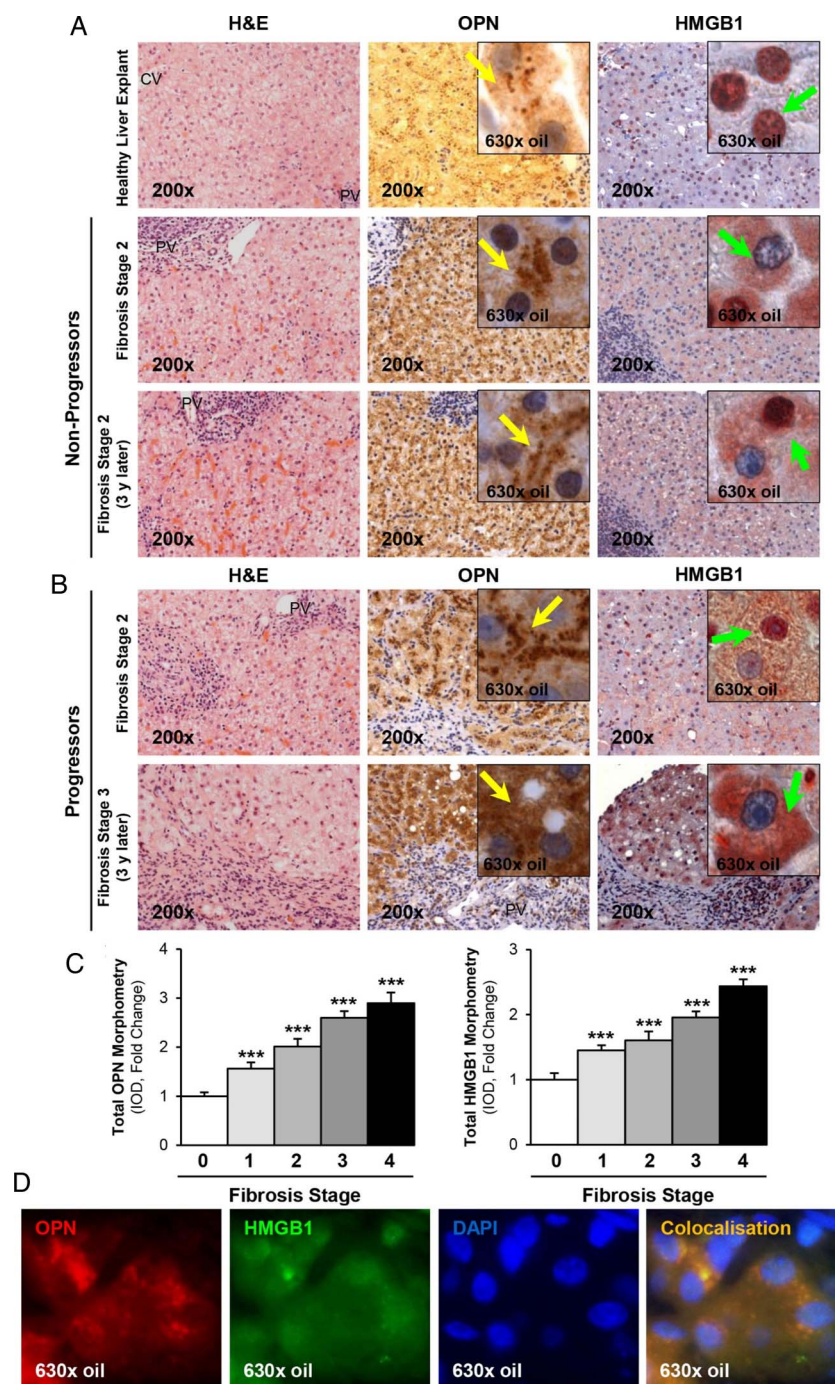
OPN and HMGB1 colocalise and their expression correlates with fibrosis progression in patients with chronic HCV-induced fibrosis

Since we hypothesised that OPN and HMGB1 could upregulate collagen-I deposition in human liver fibrosis, we determined whether there was correlation between the induction of both proteins and scarring. To this end, we analysed the expression of OPN and HMGB1 in paraffin-embedded archived human liver biopsies from deidentified controls and from patients with clinically proven hepatitis C virus (HCV). The latter were paired biopsy specimens, some of which showed progression of HCV-induced fibrosis (progressors) and others did not (non-progressors). Liver biopsies from patients with HCV showed coinduction of both OPN and HMGB1 expression compared with healthy explants (figure 1A, B). While their expression remained akin over time in the non-progressors (figure 1A), both proteins increased with fibrosis stage in the progressors (figure 1B). Computer-assisted morphometry assessment demonstrated correlation between OPN and HMGB1 expression and fibrosis stage in patients with chronic HCV infection (figure 1C). Immunofluorescence analysis proved co-localisation of both proteins in patients with chronic HCV infection (figure 1D). Thus, these results suggest that OPN and HMGB1 colocalise and their expression correlates with fibrosis progression in patients with chronic HCV-induced fibrosis.

OPN and HMGB1 colocalise and their expression correlates in CCl₄-induced liver injury in mice

To determine whether OPN is upstream of HMGB1 and dissect if OPN induces HMGB1 therefore contributing to the fibrogenic response to liver injury, we used the CCl₄ model of liver fibrosis along with genetic manipulation of *Opn* using WT, *Opn*^{−/−} and *Opn*^{Hep} Tg mice as previously.³ Immunohistochemistry (IHC) analysis revealed that CCl₄-injected *Opn*^{Hep} Tg mice showed a marked increase in hepatic OPN (figure 2A) and HMGB1 (figure 2B, top) expression compared with mineral oil (MO)-injected WT mice; however, HMGB1 immunostaining was significantly reduced in

Figure 1 Osteopontin (OPN) and high-mobility group box-1 (HMGB1) colocalise and their expression correlates with fibrosis progression in patients with chronic HCV-induced fibrosis. H&E staining, OPN and HMGB1 immunohistochemistry (IHC) in paraffin-embedded archived human liver biopsies from a deidentified control and from a patient with clinically proven hepatitis C virus (HCV)-induced fibrosis that did not progress in disease stage (stage 2) over 3 years show similar expression of OPN (yellow arrows, insets) and HMGB1 (green arrows, insets) (A). H&E staining, OPN and HMGB1 IHC from a patient with clinically proven HCV-induced fibrosis that progressed from stage 2 to 3 in 3 years show increased expression of OPN (yellow arrows, insets) and HMGB1 (green arrows, insets) (B). Total OPN and HMGB1 morphometry analysis according to fibrosis stage. Results are expressed as fold-change of the healthy liver explants, which are assigned a value of 1; n=10/group, ***p<0.001 for stages 1, 2, 3 or 4 vs 0 (C). Immunofluorescence shows colocalisation of OPN (red) and HMGB1 (green) in a patient with chronic HCV-induced fibrosis at stage 3 (D). DAPI, 4',6-diamidino-2-phenylindole; IOD, integrated optical density.



Opn^{-/-} mice, which was also quantified by morphometry analysis and western blot (figure 2B, middle). Moreover, serum HMGB1 doubled in CCl₄-injected *Opn*^{Hep} Tg compared with WT mice (not shown). Since HMGB1 nucleocytoplasmic shuttling is critical for driving downstream events,⁷ HMGB1 localisation was quantified by computer-assisted morphometry analysis. There was a significant decrease in the ratio of nuclear-to-total HMGB1 along with an increase in the ratio of cytoplasmic-to-total HMGB1 expression in CCl₄-injected *Opn*^{Hep} Tg compared with WT and it was lower in *Opn*^{-/-} mice (figure 2B, bottom). Immunofluorescence analysis demonstrated colocalisation of OPN and HMGB1 along with induced expression in CCl₄-injected WT mice (figure 2C). OPN and HMGB1 expression significantly increased in hepatocytes as shown by colocalisation with HNF4α (nuclear staining)¹² (figure 2D, top

and middle). Similarly, HMGB1 expression was enhanced in HSCs, although to a lesser extent than in hepatocytes, as shown by colocalisation with desmin (figure 2D, bottom). Furthermore, collagen-I deposition was greater in chronic CCl₄-injected *Opn*^{Hep} Tg compared with WT but it was much lesser in *Opn*^{-/-} mice as shown by IHC and morphometry analysis (figure 2E). These in vivo results suggest the possibility that OPN could drive HMGB1 release.

Hmgb1 ablation in hepatocytes partially prevents CCl₄-induced liver fibrosis in mice

Since the human and mouse data suggested a possible role for HMGB1 of hepatocyte origin in liver fibrosis, to determine the effect of blocking hepatocyte-derived HMGB1, *Hmgb1*^{ΔHep} and control littermates were chronically injected MO or CCl₄.

Figure 2 Osteopontin (OPN) and high-mobility group box-1 (HMGB1) colocalise and their expression correlates in carbon tetrachloride (CCl₄)-induced liver injury in mice. Wild-type (WT), *Opn*^{-/-} and *Opn*^{Hep Tg} mice were injected with mineral oil (MO) or CCl₄ for 1 month. OPN (A) and HMGB1 (B, top) immunohistochemistry (IHC) and morphometry analysis in livers from CCl₄-injected mice show increased OPN (yellow arrows, insets) along with HMGB1 (green arrows, insets) expression, which is greater in CCl₄-injected *Opn*^{Hep Tg} than in WT and less in *Opn*^{-/-} mice. Western blot analysis for HMGB1 in livers from MO-injected WT and CCl₄-injected WT, *Opn*^{-/-} and *Opn*^{Hep Tg} mice. The results from the western blot analysis are corrected by calnexin (loading control) (B, middle). Quantification of nuclear, cytoplasmic, nuclear-to-total and cytoplasmic-to-total HMGB1 expression (B, bottom). Immunofluorescence shows colocalisation of OPN and HMGB1 as well as induction in CCl₄-injected WT mice (C, top), which was quantified by morphometry (C, bottom). Immunofluorescence demonstrates colocalisation of OPN and HMGB1 with HNF4α (hepatocyte marker, nuclear) along with induction by CCl₄ treatment (D, top and middle). There is also colocalisation of HMGB1 with desmin (hepatic stellate cell (HSC) marker, cytoplasmic) along with induction by CCl₄ treatment (D, bottom). Collagen-I IHC and morphometry assessment in livers from MO-injected or CCl₄-injected WT, *Opn*^{-/-} and *Opn*^{Hep Tg} mice (E). In all panels, the results are expressed as fold-change of the WT mice injected MO, which are assigned a value of 1 and are mean values±SEM; n=8/group. *p<0.05, **p<0.01 and ***p<0.001 for CCl₄-injected mice versus MO-injected mice; ●p<0.05, ●●p<0.01 and ●●●p<0.001 for *Opn*^{Hep Tg} or *Opn*^{-/-} versus WT mice. CV, central vein; DAPI, 4',6-diamidino-2-phenylindole; IOD, integrated optical density; PV, portal vein.

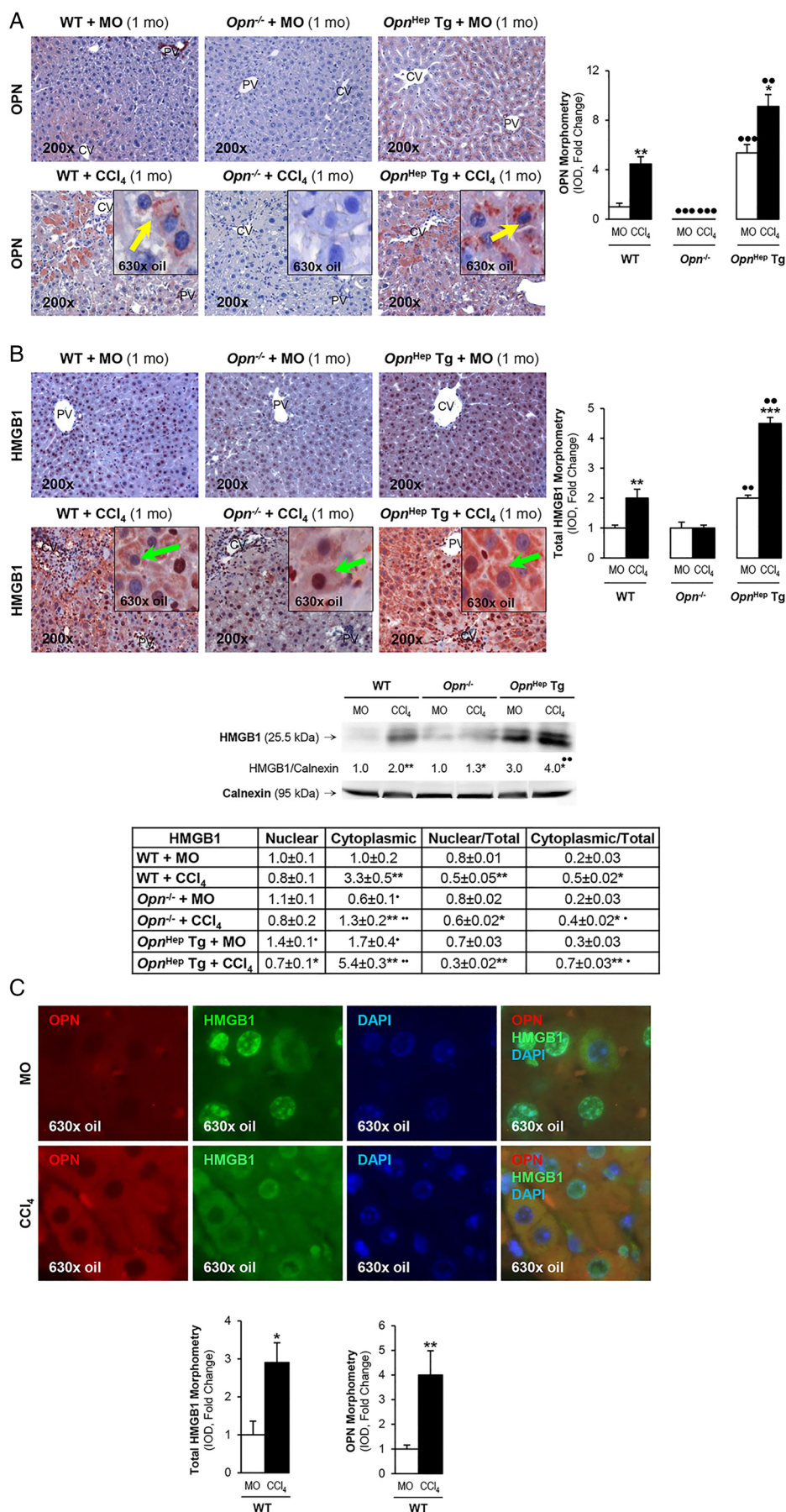
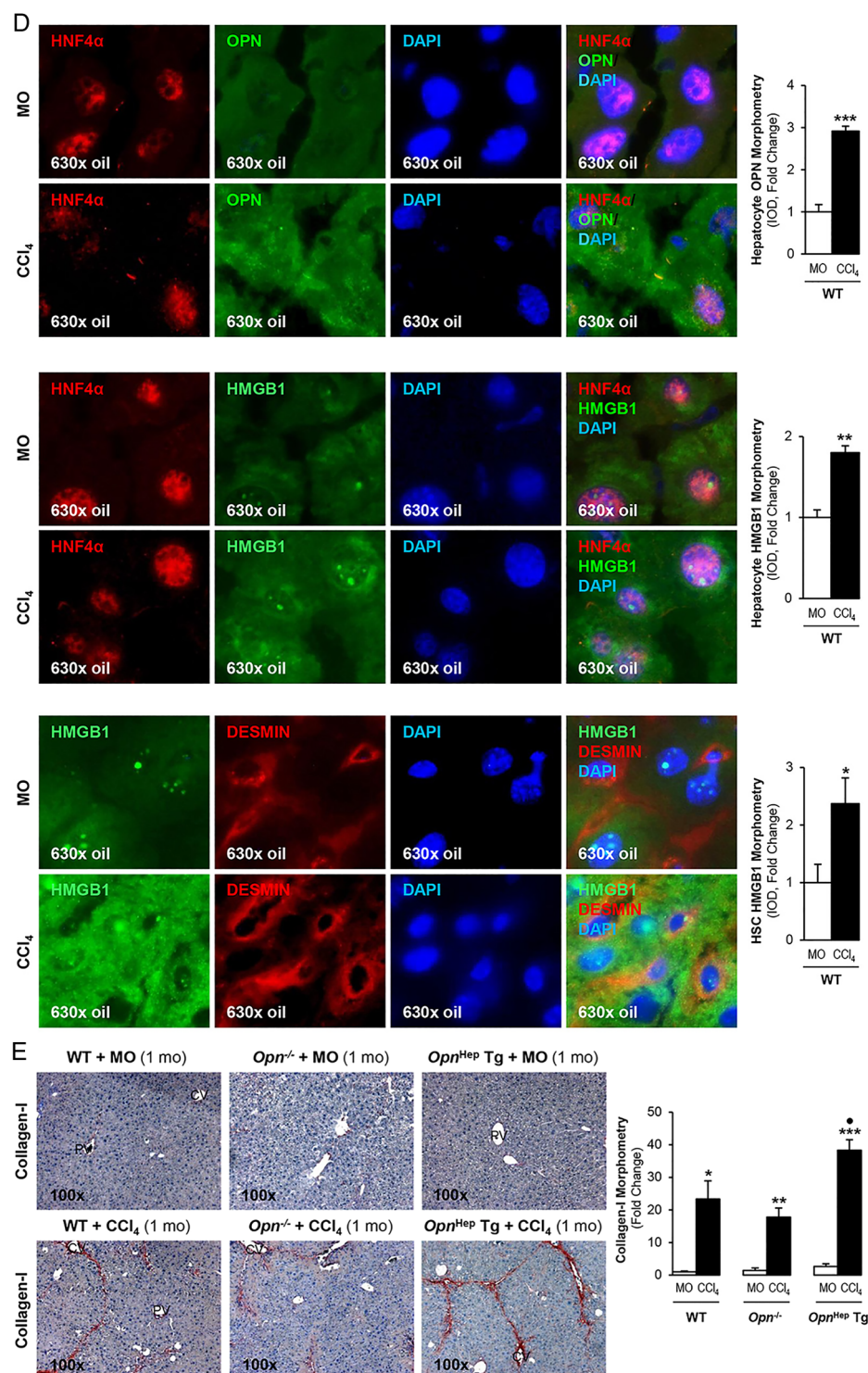


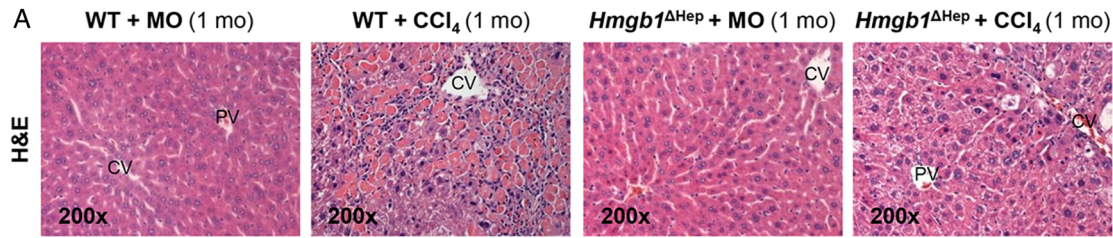
Figure 2 Continued.



H&E staining, the pathology scores and serum alanine aminotransferase plus aspartate aminotransferase activities demonstrated less necrosis, inflammation, hepatocyte ballooning degeneration and fibrosis in CCl₄-injected *Hmgb1*^{ΔHep} compared with control littermates (figure 3A). Similar results were observed in a second model of liver fibrosis induced by common bile duct ligation (BDL) (see online supplementary figure S1). *Hmgb1* deletion in hepatocytes was confirmed by IHC in livers from *Hmgb1*^{ΔHep} and control littermates (figure 3B, top). IHC revealed less collagen-I expression in CCl₄-injected *Hmgb1*^{ΔHep} compared with control littermates (figure 3B, top). *Hmgb1* ablation did not affect OPN expression

confirming that OPN is upstream of HMGB1 (figure 3B, top). The intensity of the positive staining from these proteins was quantified by morphometry analysis (figure 3B, middle). Similarly, *Hmgb1* ablation did not alter RAGE expression (figure 3B, bottom) or any other known HMGB1 receptor mRNA (not shown). Thus, *Hmgb1* ablation in hepatocytes partially prevents CCl₄-induced liver fibrosis in mice.

OPN is also upstream of HMGB1 in HSCs and they both regulate collagen-I expression in an autocrine fashion in vitro
We previously demonstrated that HSCs express OPN¹ and this study revealed that HSCs also produce HMGB1. We next asked



	Necrosis	Inflammation	Ballooning	Fibrosis
WT + MO	0±0	0.59±0.04	0.13±0.02	0±0
WT + CCl ₄	2.18±0.14***	2.93±0.16**	0.96±0.13**	2.89±0.14***
<i>Hmgb1</i> ^{ΔHep} + MO	0±0	0.38±0.03	0.1±0.01	0±0
<i>Hmgb1</i> ^{ΔHep} + CCl ₄	1.42±0.15***	1.41±0.11**	0.63±0.12**	1.72±0.17***

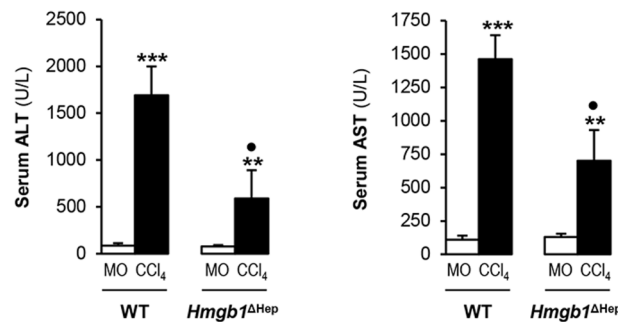


Figure 3 *Hmgb1* ablation in hepatocytes partially prevents carbon tetrachloride (CCl₄)-induced liver fibrosis in mice. *Hmgb1*^{ΔHep} and control littermates were injected mineral oil (MO) or CCl₄ for 1 month. H&E staining (A, top), the pathology scores (A, middle) and serum alanine aminotransferase (ALT) plus aspartate aminotransferase (AST) activities (A, bottom) show lower necrosis, inflammation, hepatocyte ballooning degeneration and fibrosis in *Hmgb1*^{ΔHep} compared with control littermates. High-mobility group box-1 (HMGB1); green arrows, insets and collagen-I immunohistochemistry (IHC) and morphometry analysis show reduced HMGB1 and collagen-I deposition in livers from CCl₄-injected *Hmgb1*^{ΔHep} compared with control littermates. IHC and western blot analysis demonstrate similar expression of osteopontin (OPN) and receptor for advanced glycation end-products (RAGE) in these mice (B). The results are expressed as fold-change of the MO-injected control littermates, which are assigned a value of 1 and are mean values±SEM; n=8/group. *p<0.05, **p<0.01 and ***p<0.001 for CCl₄-injected versus MO-injected mice; ●p<0.05, ●●p<0.01 and ●●●p<0.001 for *Hmgb1*^{ΔHep} versus control littermates. CV, central vein; IOD, integrated optical density; PV, portal vein; WT, wild type.

whether HSC-derived OPN could exert an autocrine effect on HMGB1 expression in HSCs and eventually on collagen-I synthesis. Freshly isolated mouse WT and *Opn*^{-/-} HSCs were evaluated for OPN, HMGB1 and collagen-I expression. *Opn*^{-/-} showed a 90% reduction in intracellular HMGB1 as well as in intracellular and extracellular collagen-I compared with WT HSCs (figure 4A, left). Conversely, WT HSCs infected with an adenovirus to overexpress OPN showed an increase in HMGB1 (figure 4A, right) and collagen-I³ expression compared with HSCs infected with control LacZ adenovirus. To determine if HMGB1 could condition OPN levels, WT and *Hmgb1*^{-/-} mouse embryonic skin fibroblasts (MEFs) were analysed for OPN, HMGB1 and collagen-I expression. *Hmgb1*^{-/-} showed similar intracellular OPN but a 90% reduction in intracellular plus extracellular collagen-I expression compared with WT MEFs (figure 4B). These data suggest that OPN is also upstream of HMGB1 in HSCs and they both regulate collagen-I expression in vitro in an autocrine fashion.

Hepatocytes are a major source of OPN and HMGB1 signalling to HSCs to increase collagen-I production

Since the human and mouse IHC suggested that hepatocytes are a major source of both OPN and HMGB1, to further define their paracrine involvement in the upregulation of collagen-I production by HSCs, cocultures of primary hepatocytes from MO-treated or CCl₄-treated mice and HSCs were established. First, the cocultures were incubated in the presence of neutralising antibodies (Abs) to OPN or HMGB1; and second, the cocultures were established with hepatocytes from MO-treated or CCl₄-treated *Opn*^{-/-}, *Hmgb1*^{ΔHep} and their respective control littermates. Western blot analysis demonstrated an increase in intracellular and extracellular collagen-I in HSCs cocultured with WT hepatocytes from CCl₄-treated mice (figure 4C, left and right, lane 3 in both blots); hence, HSCs were responsive to hepatocyte-derived factors. These mediators were identified as OPN and HMGB1, since incubation with neutralising Abs to each one of them prevented the collagen-I induction

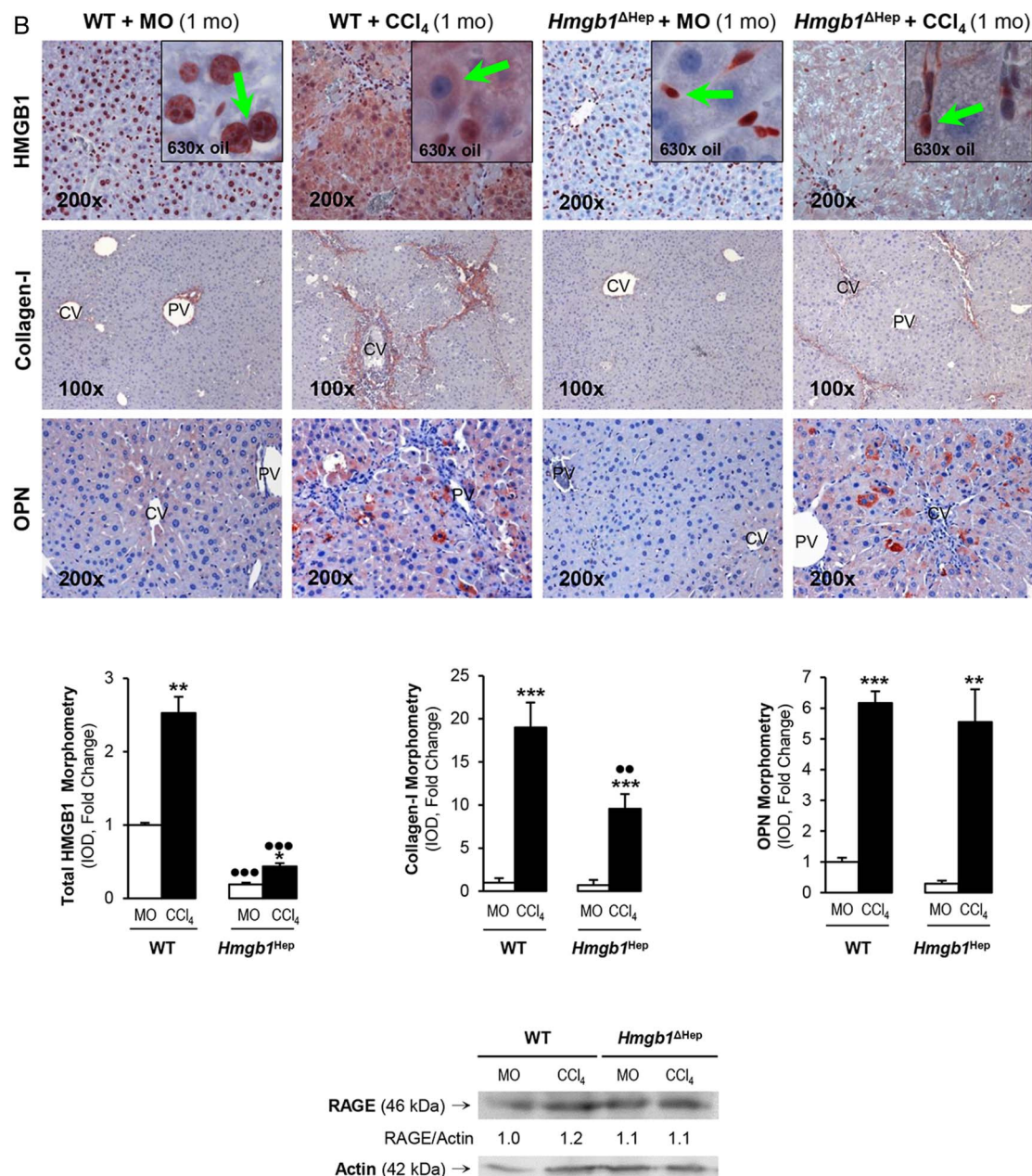


Figure 3 Continued.

in HSCs (figure 4C, left and right, lane 4 in both blots). Moreover, coculture with primary mouse hepatocytes from CCl₄-treated *Opn*^{-/-} or *Hmgb1*^{ΔHep} mice downregulated intracellular and extracellular collagen-I in HSCs and blunted the CCl₄-mediated collagen-I increase (figure 4C left and right, lane 8 in both blots). Therefore, hepatocyte-derived OPN and HMGB1 target HSCs and drive their profibrogenic behaviour.

rOPN induces HMGB1 expression and translocation in HSC and drives the increase in collagen-I production

Next, we examined if treatment with rOPN, as the upstream signal and as a surrogate of the coculture model or paracrine effects, could also replicate the increase in HMGB1 and collagen-I expression observed in HSCs. Primary rat HSCs cultured for 4 days (quiescent) or for 7 days (activated) and stimulated with rOPN increased HMGB1 and collagen-I expression (figure 5A, left). The

effects on HMGB1 were at the protein level since *Hmgb1* mRNA remained similar after the rOPN challenge (not shown) and inhibition of protein synthesis with cycloheximide blocked the increase in HMGB1 by rOPN in HSCs (figure 5A, right).

Since HMGB1 undergoes nucleocytoplasmic shuttling in response to a variety of stressors and PTMs,⁷ we next examined whether rOPN could promote HMGB1 translocation from the nucleus to the cytoplasm and eventually condition collagen-I synthesis by HSCs. Western blot analysis of nuclear and cytoplasmic proteins from HSCs stimulated with rOPN proved that the increase in cytoplasmic HMGB1 correlated with collagen-I (figure 5B). These results were also validated by immunofluorescence for HMGB1 and collagen-I in primary mouse HSCs (figure 5C).

To further confirm that following rOPN treatment, HMGB1 translocation drives collagen-I deposition, rat HSCs were

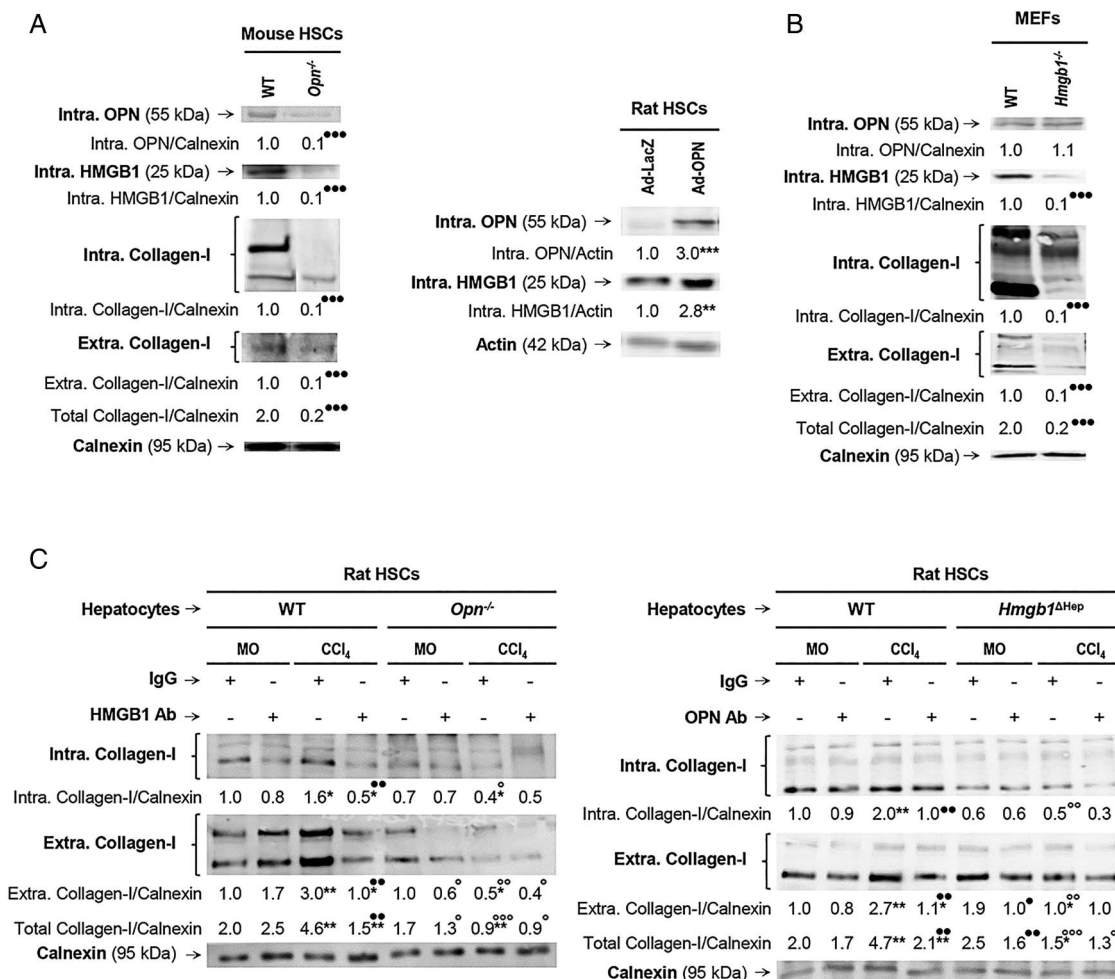


Figure 4 Osteopontin (OPN) is also upstream of high-mobility group box-1 (HMGB1) in hepatic stellate cells (HSCs) and they both regulate collagen-I expression in an autocrine fashion in vitro. Primary HSCs from wild-type (WT) and *Opn*^{-/-} mice were cultured for 5 days. Western blot analysis of intracellular OPN, HMGB1 and collagen-I plus extracellular collagen-I expression (A, left). Rat HSCs were infected with Ad-LacZ or Ad-OPN for 48 h. Western blot analysis of intracellular OPN and HMGB1 in rat HSCs infected with Ad-LacZ or Ad-OPN (A, right). Mouse embryonic skin fibroblasts (MEFs) from WT and *Hmgb1*^{-/-} mice were cultured for 1 day. Western blot analysis of intracellular OPN, HMGB1 and collagen-I plus extracellular collagen-I expression (B). Hepatocytes are a major source of OPN and HMGB1 signalling to HSCs to increase collagen-I production. Primary rat HSCs were cultured alone for 5 days and then cocultured with primary hepatocytes from mineral oil (MO)-treated or CCl₄-treated *Opn*^{-/-}, *Hmgb1*^{ΔHep} and their matching control littermates for 1 day in the presence or absence of non-immune IgG or a neutralising antibody (Ab) to HMGB1 or OPN, respectively. Western blot analysis of intracellular and extracellular collagen-I is shown (C). In all panels, the results are corrected by the specific loading control and are expressed as fold-change of the control, which are assigned a value of 1 and are mean values±SEM; n=3/group. Experiments were performed in triplicate four times. *p<0.05, **p<0.01 and ***p<0.001 for Ad-OPN or CCl₄ versus Ad-LacZ or MO; °p<0.05, °°p<0.01 and °°°p<0.001 for the *Opn*^{-/-} and *Hmgb1*^{ΔHep} coculture versus the WT and the control littermate cocultures.

transfected with constructs driving HMGB1 localisation to the nucleus or to the cytoplasm and collagen-I expression was evaluated. The constructs were (1) pGFP, an empty vector used as a negative control; (2) WT.*Hmgb1*.GFP, containing nuclear localisation signals (NLS) 1 and 2 to overexpress HMGB1 and allow response to stimuli that could drive the protein to the cytoplasm and (3) *Hmgb1*.NLS1/2(8K→8A).GFP, containing all eight lysines in the two NLS mutated to alanines that cannot be acetylated therefore resulting in HMGB1 nuclear localisation¹³ (see scheme on figure 5D).

In the absence of a stimulus, HSCs transfected with the WT.*Hmgb1*.GFP or the *Hmgb1*.NLS1/2(8K→8A).GFP vectors showed green fluorescence only in the nucleus corresponding to HMGB1 nuclear localisation (white arrows) compared with HSCs transfected with the pGFP vector, which showed diffuse green fluorescence corresponding to GFP only. Treatment with

rOPN increased collagen-I expression in WT.*Hmgb1*.GFP-transfected HSCs only (red staining); still, rOPN induced greater collagen-I expression (yellow arrows) in HSCs transfected with WT.*Hmgb1*.GFP showing cytoplasmic HMGB1 (white arrow heads) (figure 5E, top and middle panels, figure 5F). These results suggest that rOPN induces HMGB1 cytoplasmic localisation leading to an increase in collagen-I expression. Moreover, transfection with the *Hmgb1*.NLS1/2(8K→8A).GFP vector revealed that forced nuclear localisation of HMGB1 decreases the HSCs response to rOPN as less collagen-I was observed compared with the WT.*Hmgb1*.GFP-transfected HSCs (figure 5E, middle and bottom panels, figure 5F). Overall, these experiments reveal that rOPN induces HMGB1 and collagen-I expression in quiescent and activated HSCs and promotes HMGB1 translocation from the nucleus to the cytoplasm thus driving collagen-I production by HSCs; still, the mechanism for

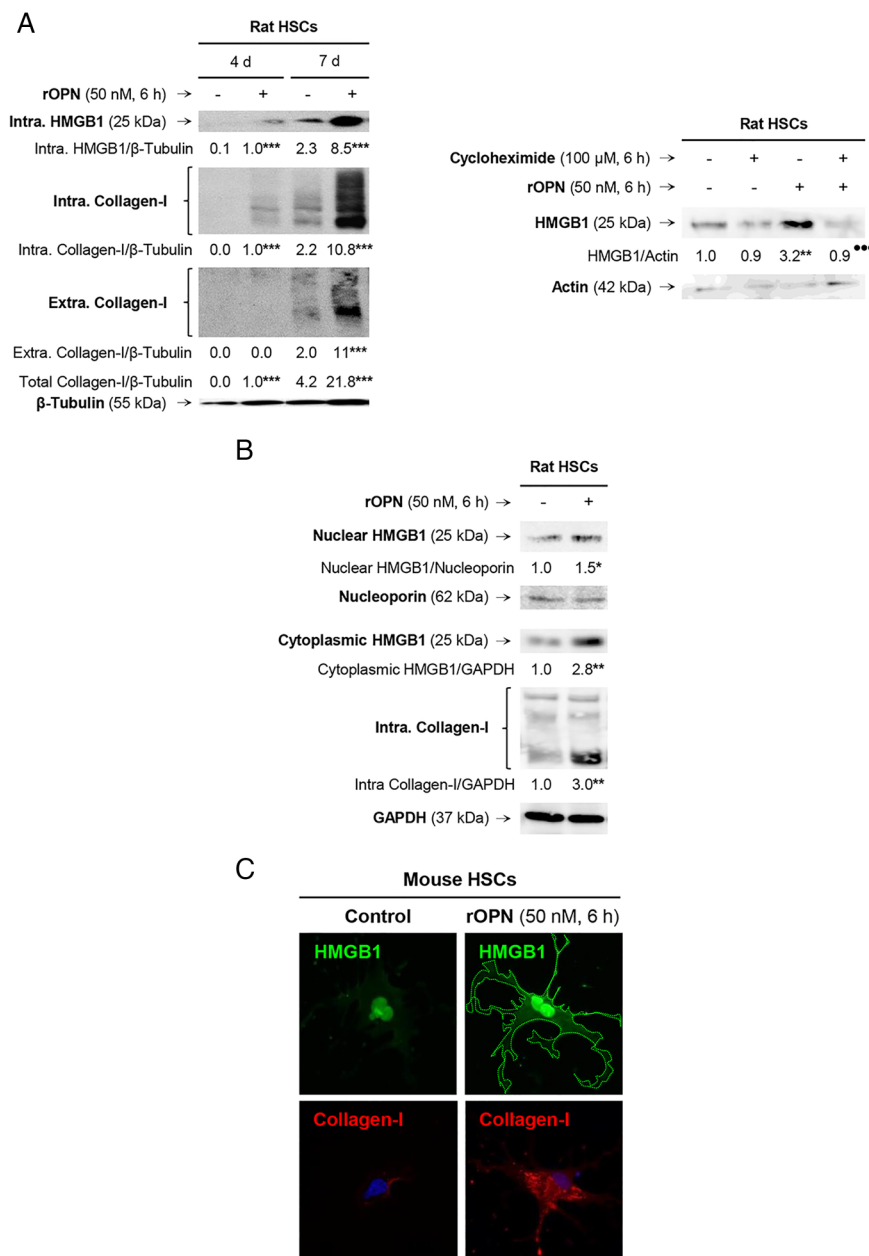


Figure 5 Recombinant osteopontin (rOPN) induces high-mobility group box-1 (HMGB1) expression and translocation in hepatic stellate cells (HSCs) and drives the increase in collagen-I production. Primary rat HSCs cultured for 4 days (quiescent) or 7 days (activated) were treated with rOPN for 6 h. Western blot analysis for intracellular HMGB1 and for intracellular plus extracellular collagen-I (A, left). Western blot analysis for HMGB1 in primary rat HSCs treated with 50 nM rOPN for 6 h in the presence or absence of 100 μ M cycloheximide (A, right). Primary rat HSCs cultured for 7 days were treated with rOPN for 6 h. Western blot analysis of nuclear plus cytoplasmic HMGB1 and intracellular collagen-I (B). In (A and B), the results are expressed as fold-change of the corresponding control, which are assigned a value of 1 if signal is present and are mean values \pm SEM; $n=3$ /group in experiments performed in triplicate four times. * $p<0.05$, ** $p<0.01$ and *** $p<0.001$ for rOPN versus control; ●●● $p<0.001$ for cycloheximide cotreated versus rOPN. Primary mouse HSCs treated with 50 nM rOPN for 6 h. Immunofluorescence analysis for HMGB1 (green) and collagen-I (red) (C). HMGB1 structure and schematic representation of the lysine residues targeted in the HMGB1 constructs (D). Rat HSCs were transfected with a series of constructs driving HMGB1 localisation followed by 0–50 nM rOPN treatment for 6 h. The constructs were (1) pGFP, an empty vector as a negative control; (2) wild-type (WT).*Hmgb1*.GFP containing nuclear localisation signals 1 (NLS1) and NLS2 to overexpress HMGB1 and (3) *Hmgb1*.NLS1/2(8K→8A).GFP containing all eight lysines in the two NLS mutated to alanines, which cannot be acetylated and result in nuclear localisation. Immunofluorescence for collagen-I (yellow arrows) and GFP fluorescence (HMGB1 localization: white arrows point at nuclear HMGB1 and white arrowheads point at cytosolic HMGB1) were visualised by confocal microscopy (E) and quantified by morphometry assessment (F). In (F), the results are expressed as fold-change of the control WT.*Hmgb1*.GFP, which are assigned a value of 1 and are mean values \pm SEM; $n=3$ /group in experiments performed in triplicate four times. * $p<0.05$, ** $p<0.01$ and *** $p<0.001$ for rOPN versus control; ●● $p<0.01$ and ●●● $p<0.001$ for *Hmgb1*(8K→8A).GFP versus WT.*Hmgb1*.GFP. IOD, integrated optical density.

Figure 5 Continued

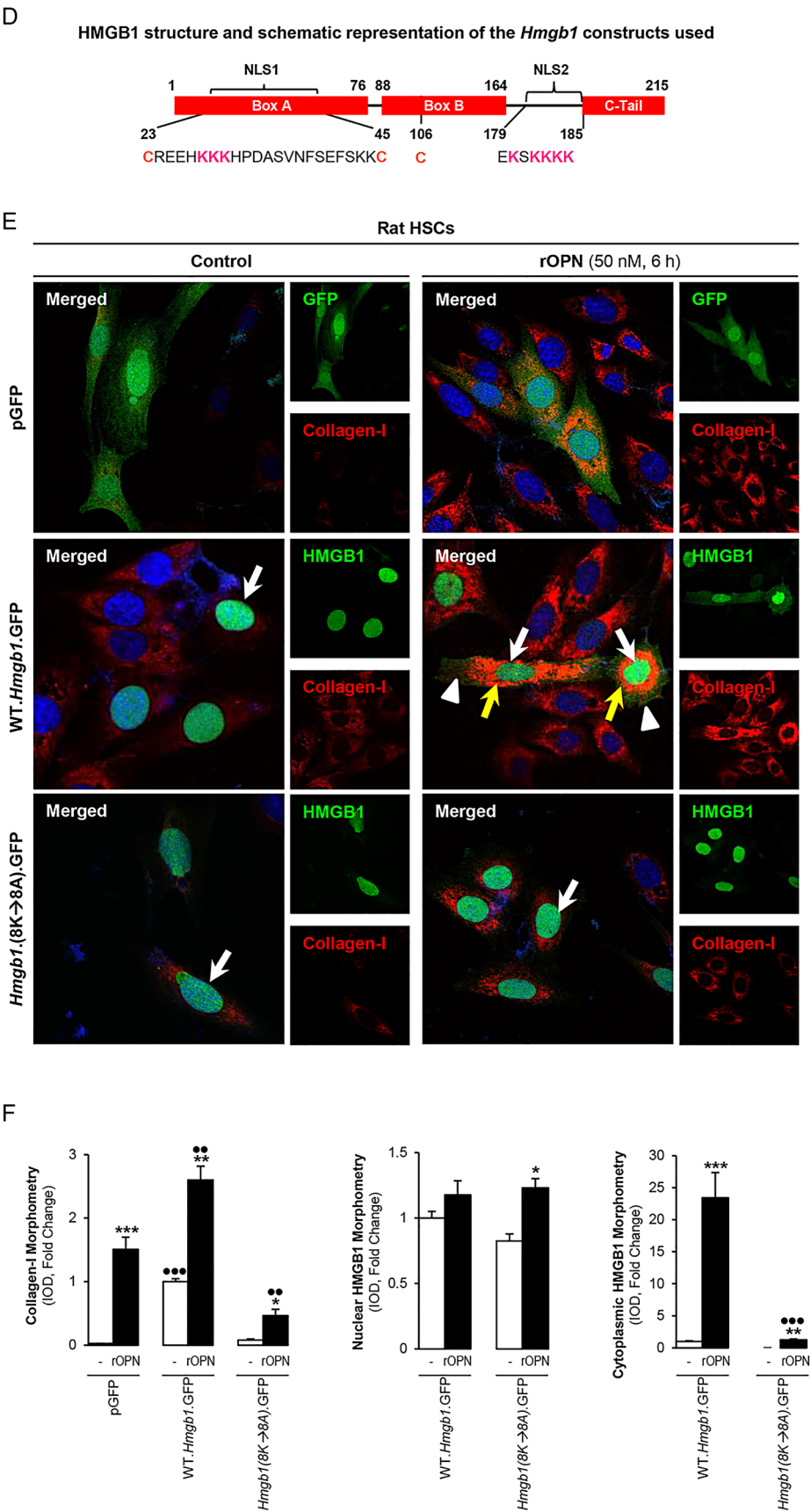
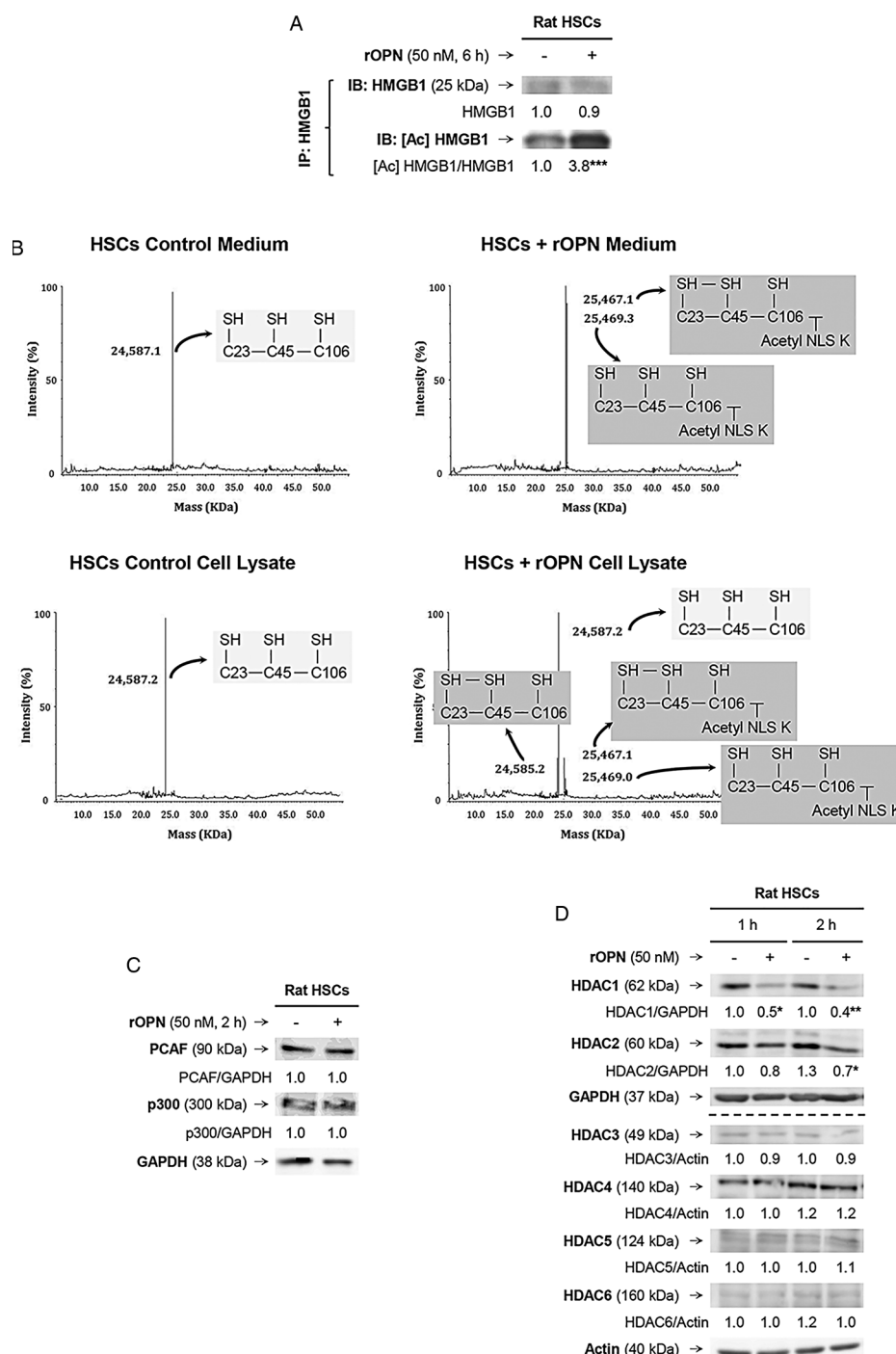


Figure 6 Recombinant osteopontin (rOPN) activates NADPH oxidase (NOX) and inhibits histone deacetylases (HDACs) 1/2 promoting high-mobility group box-1 (HMGB1) acetylation and translocation along with collagen-I upregulation in hepatic stellate cells (HSCs). Rat HSCs were treated with rOPN for 6 h. Immunoprecipitation of intracellular HMGB1 and immunoblotting for acetylated lysines (A). Identification of the HMGB1 isoforms in HSCs lysates and in the cell culture medium. Spectra of whole protein electrospray ionisation–liquid chromatography–mass spectrometry of the HMGB1 isoforms. A schematic representation of each isoform is on each spectra (grey boxes); $n=3/\text{group}$ (B). Rat HSCs were treated with rOPN for 2 h. Western blot analysis for PCAF and p300 (C). Rat HSCs were treated with rOPN for 1 and 2 h. Western blot analysis for HDACs1–6 (D). NOX activity in rat HSCs treated with rOPN for 6 h alone or pretreated for 0.5 h with apocynin or diphenyleneiodonium (DPI), the two NOX inhibitors. The percentage of dihydroethidium (DHE)-positive cells was measured by flow cytometry as an indirect measurement of O_2^- production (E). Rat HSCs were treated with rOPN for 6 h in the presence or absence of apocynin or DPI. Western blot analysis of HDACs1/2 along with intracellular and extracellular collagen-I (F). The results from the western blot analysis are corrected by the specific loading control and are expressed as fold-change of the controls, which are assigned a value of 1 and are mean values \pm SEM; $n=3/\text{group}$ in experiments performed in triplicate four times. * $p<0.05$, ** $p<0.01$ and *** $p<0.001$ for rOPN versus control; • $p<0.05$ and •• $p<0.01$ for cotreated versus rOPN. HDACs, histone deacetylases.



the mobilisation of HMGB1 in HSCs under rOPN treatment remained undefined.

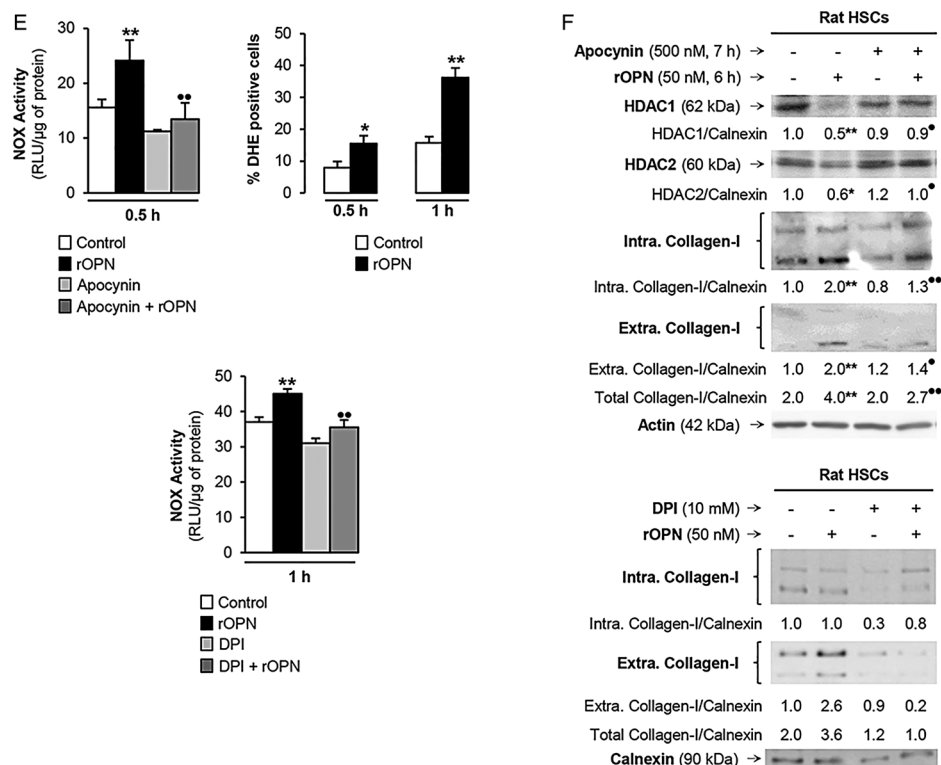
rOPN activates NOX and inhibits HDACs1/2 promoting HMGB1 acetylation and translocation along with collagen-I upregulation in HSCs

As HMGB1 nucleocytoplasmic shuttling occurs in response to stressors and/or PTMs,⁷ we examined if rOPN could trigger a specific PTM in HSCs that would increase HMGB1. Immunoprecipitation followed by immunoblotting revealed significant acetylation of HMGB1 in the presence of rOPN (figure 6A). Using electrospray ionisation–liquid chromatography–mass spectrometry,⁷ we analysed the HMGB1 residues modified under rOPN treatment in HSCs and found

significant acetylation in a cluster of eight lysines (28–30, 180 and 182–185), minimal oxidation of cysteines 23 and 45 and no phosphorylation of serine 35 (figure 6B and not shown); however, how these specific PTMs occurred remained unknown.

Acetylation typically occurs due to enhanced histone acetyltransferases (HATs) and/or decreased HDACs activity; thus, we measured the activity of HATs and HDACs. The activity of HATs remained similar; however, there was a decrease in the activity of HDACs in rOPN-treated HSCs compared with control HSCs (not shown). Although PCAF (p300/CBP-associated factor) and p300 have been described to acetylate HMGB1,¹⁴ yet, western blot analysis revealed similar PCAF and p300 expression in rOPN-stimulated HSCs compared with

Figure 6 Continued



control HSCs (figure 6C). Next, we analysed if the expression of HDACs in HSCs changed under the rOPN challenge. Western blot analysis demonstrated a decrease in HDACs1/2, whereas HDACs3–6 remained similar in rOPN-stimulated HSCs compared with control HSCs (figure 6D). Thus, rOPN acetylates HMGB1 likely by inhibiting HDACs1/2, which could contribute to HMGB1 cytoplasmic accumulation. Nevertheless, how inhibition of HDACs1/2 occurred remained undefined.

HDACs activity can be inhibited by activation of NOX with the subsequent generation of reactive oxygen species.¹⁵ To establish if rOPN could activate NOX and inhibit HDACs1/2 in HSCs, we measured NOX activity and O_2^- production and found an increase in NOX activity and O_2^- levels. When NOX induction was blocked by apocynin or diphenyleneiodonium (DPI) chloride, the two NOX inhibitors (figure 6E), they prevented the rOPN-mediated decrease in HDACs1/2 and the increase in collagen-I expression in HSCs (figure 6F). Overall, these results provide proof of concept that rOPN activates NOX to induce the production of O_2^- , which inhibits HDACs1/2 expression, allows HMGB1 acetylation and upregulates collagen-I synthesis by HSCs.

rHMGB1 signals via the PI3K–pAkt1/2/3 pathway to upregulate collagen-I expression in HSCs

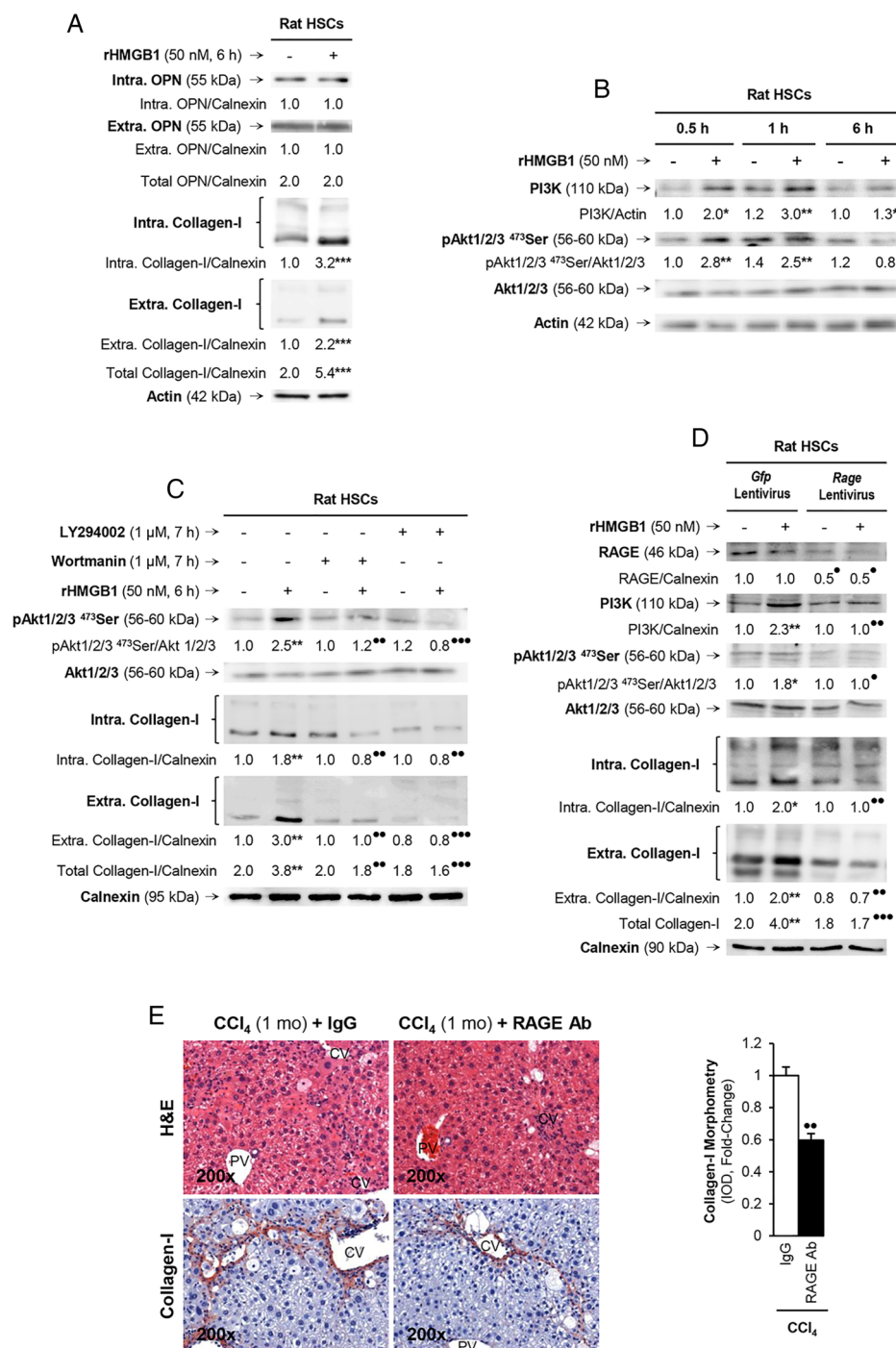
Since the human and mouse data along with the coculture studies suggested that hepatocytes produce and secrete HMGB1, which was identified as downstream of OPN, we next asked if extracellular HMGB1 per se could also signal to HSCs and increase collagen-I synthesis. To address this question, HSCs were challenged with rHMGB1, which did not alter OPN expression, yet increased intracellular and extracellular collagen-I (figure 7A). Since collagen-I production is highly dependent from protein kinase activation, to better understand how rHMGB1 upregulated collagen-I synthesis in HSCs, we analysed the expression of a series of protein kinases to determine their potential activation by rHMGB1. Following

evaluation of the expression and phosphorylation state of protein kinases known to activate collagen-I synthesis (ie, ERK1/2, PI3K, Akt, p70RSK, p38, JNK), we identified that rHMGB1 time-dependently increased PI3K and induced the phosphorylation of Akt1/2/3, its downstream target (figure 7B). To confirm that they were indeed involved in the effects of rHMGB1 on collagen-I production by HSCs, cells were preincubated with the PI3K inhibitors wortmannin or LY294002 and then challenged with rHMGB1. Western blot analysis revealed a decrease in collagen-I production under rHMGB1 treatment when cells were pretreated with inhibitor, thus validating the role of PI3K and pAkt1/2/3 in the effects of rHMGB1 on collagen-I expression in HSCs (figure 7C). Therefore, extracellular HMGB1 per se also upregulates collagen-I in HSCs via PI3K–pAkt1/2/3 signalling.

rHMGB1 signals via RAGE to upregulate collagen-I expression through the PI3K–pAkt1/2/3 pathway in HSCs

Last, since HMGB1 binds several receptors, of which RAGE¹⁶ and TLRs2/4/9^{17–19} have been described to play a role in the setting of liver fibrosis, we evaluated whether the HMGB1 effects on collagen-I were receptor-mediated. To this end, we ablated *Rage* or *Tlrs2/4/9* using shRNA lentiviral particles or siRNA strategies. Upon successful ablation (figure 7D and not shown), HSCs were treated with rHMGB1 and collagen-I expression was evaluated. RAGE (figure 7D) but not TLRs2/4/9 (see online supplementary figure S2) was critical for the effects of rHMGB1 on collagen-I upregulation in HSCs since western blot analysis showed upregulation of collagen-I following rHMGB1 treatment, without altering RAGE expression but not after *Rage* ablation (figure 7D). To identify whether the PI3K–pAkt1/2/3 signalling pathway was activated in a RAGE-dependent manner, we analysed the expression of these proteins and found no activation of PI3K and pAkt1/2/3 after rHMGB1 treatment when *Rage* was ablated (figure 7D). Overall, these results suggest that rHMGB1 signals via RAGE

Figure 7 rHMGB1 signals via receptor for advanced glycation end-products (RAGE) to upregulate collagen-I expression through the PI3K–pAkt1/2/3 pathway in hepatic stellate cells (HSCs). Rat HSCs were treated with 50 nM rHMGB1 for 6 h. Western blot analysis for intracellular plus extracellular OPN and collagen-I (A). HSCs were challenged with rHMGB1 up to 6 h and western blot analysis was performed for PI3K, pAkt1/2/3 and Akt1/2/3 (B). Western blot for pAkt1/2/3, pAkt1/2/3 and intracellular plus extracellular collagen-I in HSCs treated with rHMGB1 in the presence or absence of wortmannin or LY294002 (two PI3K inhibitors) (C). *Rage* ablation was performed in HSCs by transduction with shRNA lentiviral particles and isolation of stable clones expressing the shRNA via puromycin dihydrochloride selection. Cells were treated with rHMGB1 for 6 h followed by western blot analysis for RAGE, PI3K, pAkt1/2/3, Akt1/2/3 intracellular and extracellular collagen-I (D). The results from the western blot analysis are corrected by the specific loading control and are expressed as fold-change of the controls, which are assigned a value of 1 and are given as mean values±SEM; n=3/group in experiments performed in triplicate four times. *p<0.05, **p<0.01 and ***p<0.001 for rHMGB1 versus control; •p<0.05, ••p<0.01 and •••p<0.001 for cotreated or *Rage* ablated versus rHMGB1 or *Gfp*. Wild-type (WT) mice were injected CCl₄ for 1 month along with non-immune IgG or RAGE neutralising Ab. H&E staining and collagen-I immunohistochemistry (IHC) and morphometry analysis showing that neutralisation of RAGE protects mice from liver fibrosis (E). The results are expressed as fold-change of the IgG group, which are assigned a value of 1 and are given as mean values±SEM; n=3/group. ••p<0.01 for RAGE Ab versus IgG. CV, central vein; PV, portal vein.



and activates the PI3K–pAkt1/2/3 pathway to upregulate collagen-I in HSCs. Last, to confirm the role of RAGE in the collagen-I upregulation in liver fibrosis in vivo, WT mice were chronically injected CCl₄ in the presence of non-immune IgG or a RAGE neutralising Ab. Blockade of RAGE partially prevented liver fibrosis compared with mice injected with an irrelevant isotype-matched control monoclonal antibody (figure 7E).

DISCUSSION

Since the incidence of liver fibrosis is rising worldwide, there is a pressing need to identify novel targets and design new therapies to prevent disease onset and/or progression. To date, most of the research in this field has focused on identifying the events

involved in the pathogenesis of liver fibrosis; yet, the precise link between injured hepatocytes, HSCs and scarring remained to be identified. Thus, our goal was to dissect if OPN targets HMGB1 and how the upregulation of both proteins in hepatocytes and in HSCs contributes to the pathogenesis of liver fibrosis by regulating scarring.

This study provides compelling evidence for both co-localisation and correlation of the expression of OPN and HMGB1 with fibrosis progression in patients with clinically proven HCV-induced fibrosis.

To determine if OPN is upstream of HMGB1 and to dissect if it targets it contributing, via yet to be established mechanisms, to the fibrogenic response to liver injury, we used the CCl₄

model of liver fibrosis along with genetic manipulation of *Opn* in mice. In addition to an increase in co-localisation of OPN and HMGB1, rather remarkable in hepatocytes, their expression correlated with the extent of liver fibrosis in mice. Importantly, fibrosis was significantly greater in chronic CCl₄-injected *Opn*^{Hep} Tg compared with WT and it was much lesser in *Opn*^{-/-} mice.³ Moreover, we observed that ageing *Opn*^{Hep} Tg mice showed enhanced expression of hepatic OPN and HMGB1 and developed spontaneous fibrosis³ in the absence of a profibrogenic stimulus (see online supplementary figure S3). Overall, these in vivo results suggested that OPN is upstream of HMGB1 and that the increase in OPN, likely driving HMGB1, plays a major role in the pathogenesis of liver fibrosis in mice; yet, the specific mechanism whereby HMGB1 could act as a profibrogenic paracrine and/or autocrine DAMP remained unknown.

We have previously established two mechanisms whereby OPN contributes to liver fibrosis in vivo. Since the colocalisation studies in human and mice also suggested a possible role for hepatocyte-derived HMGB1 in liver fibrosis, next we evaluated the consequences of blocking HMGB1 in hepatocytes for the development of liver fibrosis. We demonstrated that selective ablation of *Hmgb1* in hepatocytes partially prevented CCl₄-induced liver fibrosis in mice, which was also validated in the BDL model.

To further define the paracrine involvement of hepatocyte-derived OPN and HMGB1 in the upregulation of collagen-I production by HSCs, cocultures of hepatocytes with HSCs were established. These experiments demonstrated that hepatocytes are a major source of OPN and HMGB1 in addition to a paracrine role in increasing collagen-I production by HSCs. This was further proven by the blocking effect of neutralising Abs to OPN or HMGB1 and by hepatocyte-specific ablation of *Opn* or *Hmgb1* in the cocultures. In both cases, collagen-I synthesis in HSCs was significantly reduced however far more when *Hmgb1* was ablated. Hence, hepatocyte-derived OPN and HMGB1 target HSCs and drive their profibrogenic behaviour.

Once the role of hepatocyte-derived OPN and HMGB1 was established, we then asked if intracellular OPN and HMGB1 in HSCs could also play an autocrine role driving scarring. Since we previously demonstrated that HSCs express OPN¹ and the present study revealed induction of HMGB1 under OPN treatment, we next ablated both proteins. Analysis of the autocrine effects resulting from (1) regulating *Opn* expression for HMGB1 production and (2) modulating *Hmgb1* expression for collagen-I synthesis suggested that intracellular OPN is also upstream of HMGB1 in HSCs and regulates collagen-I expression.

Next, to dissect the molecular mechanism for the paracrine effects of OPN and HMGB1 for the HSCs profibrogenic behaviour, we treated HSCs with rOPN or rHMGB1. We previously showed that rOPN upregulates collagen-I production in HSCs by binding $\alpha_v\beta_3$ integrin and activating the PI3K–pAkt1/2/3–NF κ B signalling pathway in addition to driving ductular reaction and increasing TGF- β production in biliary epithelial cells.^{1–3} Yet, in view of our data, we also considered that a downstream target of OPN, such as HMGB1, could participate in increasing collagen-I deposition thereby contributing to the pathophysiology of liver fibrosis by regulating scarring.

Extracellular OPN induced HMGB1 and collagen-I expression in quiescent and activated HSCs and also promoted HMGB1 translocation from the nucleus to the cytoplasm driving collagen-I production by HSCs as demonstrated with the transfection experiment using the constructs conditioning HMGB1 subcellular localisation in response to stimuli. The construct preventing HMGB1 acetylation in HSCs under rOPN

treatment suggested a key role of a PTM for collagen-I production in this setting. Indeed, analysis of the potential PTMs revealed extensive acetylation of HMGB1 in the cluster of eight lysines (28–30, 180 and 182–185) under OPN treatment in HSCs, which could explain the cytoplasmic increase in HMGB1 since acetylation prevents HMGB1 nuclear re-entry. To understand how this modification occurred, next we measured HATs and HDACs activity along with the expression of each of these proteins. OPN lowered HDACs1/2 activity and acetylated HMGB1 thus contributing to HMGB1 cytoplasmic localisation and increase. Furthermore, OPN activated NOX and stimulated O₂⁻ generation, which ultimately inhibited HDACs1/2 expression allowing HMGB1 acetylation and upregulating collagen-I expression in HSCs. Thus, extracellular OPN can paracrine promote the autocrine effects of HSC-derived HMGB1 in driving collagen-I deposition.

Finally, the human and mouse data along with the coculture studies suggested that hepatocytes were a major source of HMGB1, which was identified as downstream of OPN. Of note, while hepatocytes secrete a considerable amount of HMGB1,⁷ HSCs secrete it but to a much lesser degree. Next, we demonstrated that extracellular HMGB1 per se also signals to HSCs via RAGE signalling and activation of the PI3K–pAkt1/2/3 pathway to upregulate collagen-I in HSCs. Therefore, RAGE plays a major role in the HMGB1-mediated effects on collagen-I synthesis in the setting of liver fibrosis.

While the involvement of HMGB1 in other liver diseases has been reported,^{20–25} the role of HMGB1 in liver fibrosis has not been fully evaluated to date. Hence, we have identified that during the onset of liver fibrosis, the increase in OPN, and as a consequence in HMGB1, drives scarring. As proposed in this study (see online supplementary figure S4), the significant upregulation of this alarmin has critical paracrine and autocrine effects on HSCs and therefore it could be targeted to prevent or slow down the fibrogenic process.

Overall, this study challenged our current view of the mechanisms driving liver disease by reinforcing the role of hepatic OPN and HMGB1, a sterile DAMP, in the onset of liver fibrosis and tested the novel hypothesis that during fibrogenesis the increase in OPN, and as a consequence in HMGB1, acts as a paracrine and autocrine signal to trigger scarring. Development of efficient therapies for liver fibrosis must target the molecular mechanisms driving early fibrosis related to hepatocellular injury to allow rapid intervention. Importantly, HMGB1 has the advantage that, unlike other proteins, provides a wider time frame for clinical intervention due to its longer half-life.²⁶ Thus, it is an attractive target to prevent fibrosis progression. OPN and HMGB1 may also participate in other events taking place in liver fibrosis such as necrosis, inflammation and increased gut permeability. Finally, due to the extent of their production in hepatocytes, it is likely that the overall contribution of hepatocyte-derived OPN and HMGB1 to scarring is far more relevant than that of HSCs. It still remains an open question if their production in other liver cells or in other organs is also relevant or perhaps synergistic for liver fibrosis and if specific PTMs of HMGB1 could also condition the noxious effects of HMGB1 in the liver environment.

Correction notice This article has been corrected since it published Online First. The Open Access licence has been added.

Acknowledgements The authors are very grateful to Drs David T Denhardt (Rutgers University, New Brunswick, New Jersey, USA) for his generous gift of the 2A1 and 2C5 Abs, Marco E. Bianchi (San Raffaele University, Milan, Italy) for providing the *Hmgb1* mutants, Timothy R. Billiar (University of Pittsburgh, Pittsburgh, Pennsylvania, USA) for donating the *Hmgb1*^{fl/fl} and Satoshi Mochida

(Saitama Medical University, Saitama, Japan) for providing the *Opn*^{Hep} Tg mice. We are also very thankful to all past and current members from the Nieto Laboratory for their helpful comments and suggestions throughout the course of this project. Confocal microscopy was performed at the Microscopy Shared Resource Facility at the Icahn School of Medicine at Mount Sinai.

Contributors EA and XG performed in vitro and in vivo experiments and edited the manuscript. T-ML, FM, AL, YL, NK and RU performed some experiments and edited the manuscript. NT provided the human samples and edited the manuscript. DJA performed the analysis of the HMGB1 isoforms and edited the manuscript. NN directed the project, drafted and edited the manuscript and obtained funding.

Funding Short-term Bancaja Fellowship and Postdoctoral Fellowship from the Asociación Española para el Estudio del Hígado, Spain (EA). Postdoctoral fellowships from the Basque Government (Spain) (AL), Keio University School of Medicine (Japan) (NK) and the Government of Navarre, Spain (RU). Wellcome Trust research fellowship (DJA) and support from the Medical Research Council Centre for Drug Safety Science (DJA and NN). UK regenerative medicine platform (UKRMP) (DJA and NN). US Public Health Service Grants R01 DK069286, R56 DK069286 and R56 DK069286-06S1 from the National Institute of Diabetes and Digestive and Kidney Diseases (NN). US Public Health Service Grants P20 AA017067, P20 AA017067-01S1, P20 AA017067-03S1 and U01 AA021887 from the National Institute on Alcohol Abuse and Alcoholism (NN).

Competing interests None declared.

Patient consent Obtained.

Ethics approval IRB.

Provenance and peer review Not commissioned; externally peer reviewed.

Open Access This is an Open Access article distributed in accordance with the terms of the Creative Commons Attribution (CC BY 4.0) license, which permits others to distribute, remix, adapt and build upon this work, for commercial use, provided the original work is properly cited. See: <http://creativecommons.org/licenses/by/4.0/>

REFERENCES

- Wang X, Lopategi A, Ge X, et al. Osteopontin induces ductular reaction contributing to liver fibrosis. *Gut* 2014;63:1805–18.
- Leung TM, Wang X, Kitamura N, et al. Osteopontin delays resolution of liver fibrosis. *Lab Invest* 2013;93:1082–9.
- Urtasun R, Lopategi A, George J, et al. Osteopontin, an oxidant stress sensitive cytokine, up-regulates collagen-I via integrin $\alpha(V)\beta(3)$ engagement and PI3K/pAkt/NF κ B signaling. *Hepatology* 2012;55:594–608.
- Kang HJ, Lee H, Choi HJ, et al. Non-histone nuclear factor HMGB1 is phosphorylated and secreted in colon cancers. *Lab Invest* 2009;89:948–59.
- Taira J, Kida Y, Kuwano K, et al. Protein phosphatase 2A dephosphorylates phosphoserines in nucleocytoplasmic shuttling and secretion of high mobility group box 1. *J Biochem* 2013;154:299–308.
- Bianchi ME, Manfredi AA. High-mobility group box 1 (HMGB1) protein at the crossroads between innate and adaptive immunity. *Immunol Rev* 2007;220:35–46.
- Ge X, Antoine DJ, Lu Y, et al. High mobility group box-1 (HMGB1) participates in the pathogenesis of alcoholic liver disease (ALD). *J Biol Chem* 2014;289:22672–91.
- Scaffidi P, Misteli T, Bianchi ME. Release of chromatin protein HMGB1 by necrotic cells triggers inflammation. *Nature* 2002;418:191–5.
- Albayrak A, Uyanik MH, Cerrah S, et al. Is HMGB1 a new indirect marker for revealing fibrosis in chronic hepatitis and a new therapeutic target in treatment? *Viral Immunol* 2010;23:633–8.
- Mochida S, Yoshimoto T, Mimura S, et al. Transgenic mice expressing osteopontin in hepatocytes as a model of autoimmune hepatitis. *Biochem Biophys Res Commun* 2004;317:114–20.
- Huang H, Nace GW, McDonald KA, et al. Hepatocyte-specific high-mobility group box 1 deletion worsens the injury in liver ischemia/reperfusion: a role for intracellular high-mobility group box 1 in cellular protection. *Hepatology* 2014;59:1984–97.
- Yamanishi K, Doe N, Sumida M, et al. Hepatocyte nuclear factor 4 alpha is a key factor related to depression and physiological homeostasis in the mouse brain. *PLoS One* 2015;10:e0119021.
- Bonaldi T, Talamo F, Scaffidi P, et al. Monocytic cells hyperacetylate chromatin protein HMGB1 to redirect it towards secretion. *EMBO J* 2003;22:5551–60.
- Pasheva E, Sarov M, Bidjekov K, et al. In vitro acetylation of HMGB-1 and -2 proteins by CBP: the role of the acidic tail. *Biochemistry* 2004;43:2935–40.
- He M, Zhang B, Wei X, et al. HDAC4/5-HMGB1 signalling mediated by NADPH oxidase activity contributes to cerebral ischaemia/reperfusion injury. *J Cell Mol Med* 2013;17:531–42.
- Goodwin M, Herath C, Jia Z, et al. Advanced glycation end products augment experimental hepatic fibrosis. *J Gastroenterol Hepatol* 2013;28:369–76.
- Miura K, Yang L, van Rooijen N, et al. Toll-like receptor 2 and palmitic acid cooperatively contribute to the development of nonalcoholic steatohepatitis through inflammasome activation in mice. *Hepatology* 2013;57:577–89.
- Vespasiani-Gentilucci U, Carotti S, Perrone G, et al. Hepatic toll-like receptor 4 expression is associated with portal inflammation and fibrosis in patients with NAFLD. *Liver Int* 2015;35:569–81.
- Miura K, Kodama Y, Inokuchi S, et al. Toll-like receptor 9 promotes steatohepatitis by induction of interleukin-1 β in mice. *Gastroenterology* 2010;139:323–34.e7.
- Tsung A, Klune JR, Zhang X, et al. HMGB1 release induced by liver ischemia involves Toll-like receptor 4 dependent reactive oxygen species production and calcium-mediated signaling. *J Exp Med* 2007;204:2913–23.
- Martin-Murphy BV, Holt MP, Ju C. The role of damage associated molecular pattern molecules in acetaminophen-induced liver injury in mice. *Toxicol Lett* 2010;192:387–94.
- Li X, Wang LK, Wang LW, et al. Cisplatin protects against acute liver failure by inhibiting nuclear HMGB1 release. *Int J Mol Sci* 2013;14:11224–37.
- Majumdar M, Ratho R, Chawla Y, et al. High levels of circulating HMGB1 as a biomarker of acute liver failure in patients with viral hepatitis E. *Liver Int* 2013;33:1341–8.
- Wang W, Sun L, Deng Y, et al. Synergistic effects of antibodies against high-mobility group box 1 and tumor necrosis factor- α antibodies on D-(+)-galactosamine hydrochloride/lipopolysaccharide-induced acute liver failure. *FEBS J* 2013;280:1409–19.
- Antoine DJ, Williams DP, Kipar A, et al. Diet restriction inhibits apoptosis and HMGB1 oxidation and promotes inflammatory cell recruitment during acetaminophen hepatotoxicity. *Mol Med* 2010;16:479–90.
- Wang H, Bloom O, Zhang M, et al. HMGB-1 as a late mediator of endotoxin lethality in mice. *Science* 1999;285:248–51.

Correction: Signally via the osteopontin and high mobility group box-1 axis drives the fibrogenic response to liver injury

Arriazu E, Ge X, Leung T-M, *et al.* Signally via the osteopontin and high mobility group box-1 axis drives the fibrogenic response to liver injury. *Gut* 2017;66:1123–37. doi: 10.1136/gutjnl-2015-310752.

Panel B in figure 6 is incorrect and has been removed. The updated figure and legend should be:

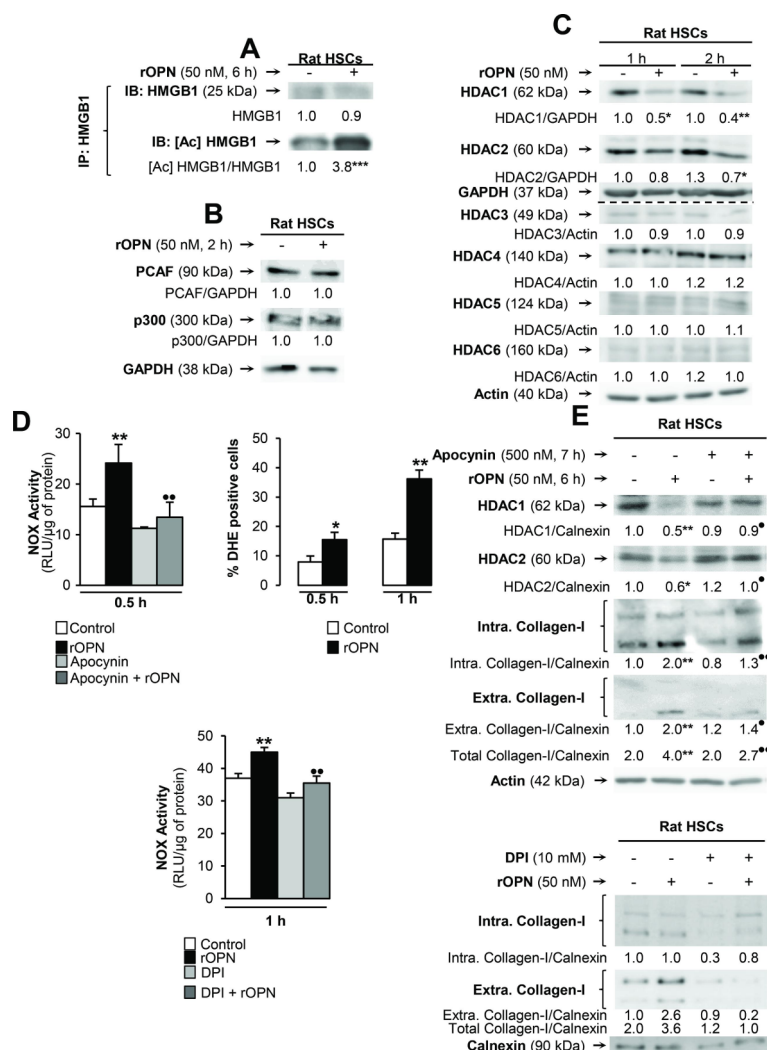


Figure 6 rOPN activates NOX and inhibits HDACs1/2 promoting HMGB1 acetylation and translocation along with collagen-I up-regulation in HSCs. Rat HSCs were treated with rOPN for 6 h. Immunoprecipitation of intracellular HMGB1 and immunoblotting for acetylated lysines (A). Rat HSCs were treated with rOPN for 2 h. Western blot analysis for PCAF and p300 (B). Rat HSCs were treated with rOPN for 1 and 2 h. Western blot analysis for HDACs1-6 (C). NOX activity in rat HSCs treated with rOPN for 6 h alone or pretreated for 0.5 h with apocynin or DPI, two NOX inhibitors. The percentage of DHE positive cells was measured by flow cytometry as an indirect measurement of O_2^- production (D). Rat HSCs were treated with rOPN for 6 h in the presence or absence of apocynin or DPI. Western blot analysis of HDACs1/2 along with intra- and extracellular collagen-I (E). The results from the western blot analysis are corrected by the specific loading control and are expressed as fold-change of the controls, which are assigned a value of 1 and are mean values \pm SEM; n=3/group in experiments performed in triplicate four times. * P <0.05, ** P <0.01 and *** P <0.001 for rOPN versus control; • P <0.05 and •• P <0.01 for co-treated versus rOPN.



OPEN ACCESS

Open access This is an open access article distributed in accordance with the Creative Commons Attribution Non Commercial (CC BY-NC 4.0) license, which permits others to distribute, remix, adapt, build upon this work non-commercially, and license their derivative works on different terms, provided the original work is properly cited, appropriate credit is given, any changes made indicated, and the use is non-commercial. See: <http://creativecommons.org/licenses/by-nc/4.0/>.

© Author(s) (or their employer(s)) 2020. Re-use permitted under CC BY-NC. No commercial re-use. See rights and permissions. Published by BMJ.

Gut 2020;**69**:e2. doi:10.1136/gutjnl-2015-310752corr1



Check for updates

SUPPLEMENTARY MATERIAL

SUPPLEMENTARY MATERIAL AND METHODS

General methodology. Details on general methodology such as ALT and AST activities, H&E staining, OPN, HMGB1 and collagen-I IHC, western blot, DHE, adenoviral infection, mRNA isolation and qPCR for genotyping are described in previous publications from our laboratory [1, 2, 3]. The source of commercially available Abs used in the western blot analysis can be found in Supplementary Table 1. The mouse embryonic skin fibroblast (MEF) cell line was obtained from HMGBiotech (Milan, Italy). Primary hepatocytes from WT, *Opn*^{-/-} and *Hmgb1*^{ΔHep} mice injected with either MO or CCl₄; primary HSCs from WT and *Opn*^{-/-} mice and primary rat HSCs were isolated and co-cultured as previously [3, 4]. Nuclear and cytoplasmic proteins were extracted according to the method of Dignam *et al* [5]. Silencing of *Rage* and *Tlrs2/4/9* was performed using conventional siRNA transfection (*Rage* [sc-106985], *Tlr4* [sc-15001] and *Tlr9* [sc-270187] were from Santa Cruz Biotechnology (Santa Cruz, CA); *Tlr2* [sc160440] was from Life Technologies (Carlsbad, CA). ShRNA lentiviral particles to silence *Rage* and *Gfp*, the latter used as control, were from Santa Cruz Biotechnology.

Human samples. Dr. Theise provided paraffin-embedded archived human liver biopsies from de-identified controls (healthy liver explants) and from post-transplant patients with clinically proven HCV-induced fibrosis scored according to the modified Ishak staging for fibrosis which also parallels the Metavir staging system [6]. Even if nowadays is not the standard of care, it was at the time of sample collection. Biopsies were repeated after several years without treatment to evaluate for progression and a new need to treat. These archived samples were IRB approved and no patient information was disclosed.

Induction of liver injury. 10-wks old male WT, *Opn*^{-/-} and *Opn*^{Hep} Tg littermates, *Hmgb1*^{ΔHep} and control littermates were used. We used the CCl₄ and the BDL well-established models of

liver fibrosis. In the CCl₄ model, mice were i.p. injected twice a wk with 0.5 ml/kg b. wt. of CCl₄ or equal volume of mineral oil (MO) for 1 mo and they were sacrificed 48 h after the last CCl₄ injection to avoid an acute-phase response over chronic liver injury. In one experiment, mice were co-treated with non-immune IgG or RAGE neutralizing Ab i.p. injected 1 h before every CCl₄ injection for 1 mo. In the BDL model, *Hmgb1*^{ΔHep} and control littermates underwent ligation of the common bile duct to induce cholestasis or sham operation (control) and were sacrificed 2 wks later. A set of WT and *Opn*^{Hep} Tg mice was allowed to age for 1 yr and samples were collected for analysis of spontaneous fibrogenesis.

Pathology. In all experiments, the entire left mouse liver lobe was collected and fixed in 10% neutral-buffered formalin and processed into paraffin sections for H&E or IHC. The scores for centrilobular necrosis were 1 = hepatocyte necrosis affecting only zone 3, 2 = in addition to zone 3 necrosis, occasional bridging necrosis was seen and 3 = pronounced bridging and confluent necrosis. Inflammation was noted to be lymphocytes present in the lobules and were scored as follows: 1 = rare foci, 2 = up to 5 foci and 3 when there were >5 foci. Ballooning degeneration was identified when hepatocytes were enlarged in most cases to more than twice the size of its neighboring cells. In addition, the cytoplasmic membrane became rounded instead of the usual hexagonal shape of normal hepatocytes. Most of the cytoplasm appeared empty except for a few irregular wisps of pink material representing damaged cytoplasmic content. The degree of fibrosis ranged from 0 to 4 and patterned after the Brunt system [7]. Briefly, it was as follows: 1 = perisinusoidal/perivenular fibrosis alone, 2 = perisinusoidal/perivenular fibrosis plus portal fibrosis, 3 = bridging fibrosis and 4 = cirrhosis. In the BDL model, ductular reaction was noted to be proliferation of bile ductules at the margins of the portal tracts and the score was 1 = rare bile ductules present, 2 = irregular buds of bile ductules affecting some portal tracts and 3 = when bile ductules are more prominent and affect the majority of portal areas and/or strings of bile ductular epithelial cells were seen intermingled

with hepatocytes. The assessment of the above scores was uniformly performed under 100x magnification.

Immunohistochemistry. The 2A1 OPN Ab was used on IHC and on immunofluorescence. The collagen-I Ab was from Chemicon International (Billerica, MA) and was used on IHC. The HMGB1 Ab was from Abcam and was used on IHC and on immunofluorescence. Specificity of the OPN and HMGB1 Abs was validated using *Opn*^{-/-} and *Hmgb1*^{ΔHep} mice, respectively (not shown). The HNF4α and the desmin Abs were from Santa Cruz Biotechnology. In the IHC, reactions were developed using the Histostain Plus detection system (Life Technologies, Waltham, MA). For the OPN, HMGB1 and collagen-I IHC computer-assisted morphometry assessment, the integrated optical density (IOD) was calculated from 10 random fields per section containing similar size portal tracts and central veins at 100x and using Image-Pro 7.0 Software (Media Cybernetics, Bethesda, MD). The results were averaged and expressed as fold-change of the controls. To quantify the cellular localization of HMGB1, the intensity of the red area corresponding to HMGB1 positive staining in the scanned fields was averaged and considered the total HMGB1 positive staining. Next, the software was set to select all nuclei and the intensity of the stained red area corresponding to HMGB1 nuclear positive staining in the scanned fields was averaged and considered the nuclear HMGB1 staining. The nuclear staining was then subtracted from the total staining to calculate the cytoplasmic HMGB1 staining. The results were averaged and expressed as fold-change of the controls. The HMGB1 expression ratios were calculated by morphometry analysis as above in 20 fields per slide at 200x magnification and are expressed as nuclear-to-total and as cytoplasmic-to-total HMGB1 expression.

Cell treatments. Due to the almost full homology of *Hmgb1* and *Opn* between rat and mice, in the majority of the experiments we used primary rat HSCs due to their greater abundance.

Primary rat (250,000 cells/well) or mouse (10,000 cells/well) HSCs were seeded on 6-well or 12-well plates in DMEM/F12 with 10% FBS. Cells were cultured using DMEM-F12 for 4 to 7 d, which was replaced by serum-free DMEM-F12 prior to either endotoxin-free human rOPN treatment (1433-OP-050/CF, R&D Systems, Minneapolis, MN) or rHMGB1 (1690-HM, R&D Systems). Time-course (5 min-48 h) and dose-response (5-500 nM) experiments along with viability assays were carried out to determine the final concentration of rOPN and of rHMGB1 (both at 50 nM) and the best time-point for collagen-I induction (both at 6 h). *Hmgb1*^{-/-} MEFs were used since *Hmgb1*^{-/-} mice are embryonically lethal and HSCs cannot be isolated from them; yet, they have similar phenotype than HSCs. The following treatments were added to the cells 1 h prior to incubation with rOPN and rHMGB1: 0.5 μM wortmannin (Calbiochem, San Diego, CA), 0.5 μM LY294002 (Cell Signaling, Danvers, MA), 0.5 μM apocynin (Fluka, St. Louis, MO), 0.5 μM diphenyleneiodonium chloride (Sigma, St. Louis, MO) or 100 μM cycloheximide (Sigma). The following neutralizing antibodies were added to the cells for 6 h: 5 μg/ml HMGB1 Ab (Shino-Test, Tokyo, Japan) or 5 μg/ml OPN Ab clone 2C5 (provided by Dr. David T. Denhardt). Co-cultures of hepatocytes and HSCs were established as described in earlier publications [4, 8, 9].

Immunofluorescence. Primary mouse HSCs (1,000 cells/well) were seeded in DMEM/F12 with 10% FBS on 12-well plates containing round cover slips on the bottom of the wells. The medium was replaced by serum-free DMEM/F12 overnight prior to the specific treatments following which the cells were gently rinsed with 1x PBS, fixed with 4% paraformaldehyde and permeabilized with 0.5% Triton X-100. After blocking with 5% FBS, the primary Abs used were HMGB1 (Abcam, Cambridge, MA) and collagen-I (Millipore, Billerica, MA) and then the Alexa-488 conjugated goat anti-mouse IgG and Alexa-568 conjugated goat anti-mouse IgG (Life Technologies). Images were acquired by confocal microscopy using a 630x 1.4NA with immersion oil objective at our Microscopy Shared Resource Facility.

Analysis of serum and liver HMGB1 by ESI-LC-MS. All chemicals and solvents used were of the highest available grade (Sigma). Samples were pre-cleared with 50 μ l protein G-Sepharose beads for 1 h at 4°C. HMGB1 present in serum or liver was immunoprecipitated with 5 μ g of rabbit anti-HMGB1 for 16 h at 4°C as previously described [10]. For the analysis of HMGB1 PTMs, free thiol groups within HMGB1 were alkylated for 90 min with 10 mM iodoacetamide at 4°C. Cysteine residues in disulfide bonds were then reduced with 30 mM dithiothreitol at 4°C for 1 h followed by alkylation of newly exposed thiol groups with 90 mM NEM at 4°C for 10 min. Samples were subjected to trypsin (Promega, Madison, WI) or GluC (New England Biolabs, Ipswich, MA) digestion according to manufacturer's instructions and de-salted using C18 zip-tips (Millipore). Characterization of whole protein molecular weights, acetylated lysine residues or redox modifications on cysteine residues within HMGB1 were determined as described previously by whole protein ESI or tandem mass spectrometry (MS/MS) [11, 12, 13] using either an AB Sciex QTRAP 5500 or an AB SciexTripleTOF 5600 (Sciex Inc., Framingham, MA). Peptide analysis was determined using an AB Sciex QTRAP 5500 equipped with a NanoSpray II source by in-line liquid chromatography using a U3000 HPLC System (Dionex, CA), connected to a 180 μ m by 20 mm nanoAcquity UPLC C₁₈ trap column and a 75 μ m by 15 cm nanoAcquity UPLC BEH130 C₁₈ column (Waters, Milford, MA) via reducing unions. A gradient from 0.05% TFA (v/v) to 50% ACN/0.08% TFA (v/v) in 40 min was applied at a flow rate of 200 nL/min. The ion spray potential was set to 2,200-3,500 V, the nebulizer gas to 19 and the interface heater to 150°C.

Vectors transfection. The following vectors were used in the transfection studies: 1) pGFP, an empty vector to serve as a negative control; 2) *Hmgb1*.WT.GFP, containing NLS1 and NLS2 to overexpress HMGB1 and allow response to stimuli that could drive the protein to the cytoplasm;

and 3) *Hmgb1*.NLS1/2(8K→8A).GFP, containing all 8 lysines in the two NLS mutated to alanines and that cannot be acetylated hence resulting in nuclear HMGB1 localization. These mutants were provided by Dr. Marco E. Bianchi (San Raffaele University, Milan, Italy) [14]. HSCs were transfected with these vectors using Lipofectamine 2000 (Life Technologies) as a carrier for 48 h and then treated with rOPN for 6 h.

NOX oxidase activity. HSCs were subjected to three freeze-thaw cycles in 50 mM phosphate buffer containing 1 mM EGTA, 150 mM sucrose and a cocktail of protease inhibitors at pH 7.4. NOX activity was measured using the indirect lucigenin-derived chemiluminescence method [15]. The reaction was initiated by adding 100 µg of protein to 100 µl of reaction buffer containing 100 µM NADPH and 5 µM lucigenin. Luminescence was recorded every 3 min over a period of 20 min in a luminescence reader.

IP:IB. 100 µg of total protein were incubated with 1 µg of HMGB1 Ab for 1 h at 4°C in a rocking device to enable binding between the protein and the Ab. Then, 20 µl of protein A/G PLUS-Agarose (Santa Cruz Biotechnology) were added and incubated for 3 h at 4°C in a rocking device. Samples were washed three times with RIPA buffer and spun down at 12,000 rpm for 2 min. Samples were resuspended in 20 µl of loading buffer, boiled for 7 min and spun down at 12,000 rpm for 2 min. The supernatant was analyzed for acetylated lysines and HMGB1 loading by western blot.

SUPPLEMENTARY RESULTS

***Hmgb1* ablation in hepatocytes partially prevents BDL-induced liver fibrosis in mice.**

Hmgb1^{ΔHep} and control littermates were subjected to BDL. H&E staining and the pathology scores demonstrated less necrosis, inflammation, hepatocyte ballooning degeneration and fibrosis in BDL *Hmgb1*^{ΔHep} compared to control littermates (Supplementary Figure 1A, top and Supplementary Figure 1B). *Hmgb1* deletion in hepatocytes was confirmed by IHC in livers from *Hmgb1*^{ΔHep} and control littermates and IHC revealed less collagen-I expression in CCl₄-injected *Hmgb1*^{ΔHep} compared to control littermates (Supplementary Figure 1A, middle). *Hmgb1* ablation did not affect OPN expression confirming that OPN is upstream of HMGB1 (Supplementary Figure 1A, bottom).

rHMGB1 signals via RAGE to up-regulate collagen-I expression in HSCs. Last, since HMGB1 binds several receptors, of which RAGE [16] and TLRs2/4/9 [17, 18, 19] have been described to play a role in the setting of liver fibrosis, we evaluated whether the HMGB1 effects on collagen-I were receptor-mediated. To this end, we ablated *Rage* or *Tlrs2/4/9* using siRNA. HSCs were treated with rHMGB1 and collagen-I expression was evaluated. RAGE but not TLRs2/4/9 was critical for the effects of rHMGB1 on collagen-I up-regulation in HSCs since western blot analysis showed up-regulation of collagen-I following rHMGB1 treatment but not after *Rage* ablation (Supplementary Figure 2).

Aging *Opn*^{Hep} Tg mice show elevated HMGB1 expression and develop spontaneous fibrosis. We previously showed that *Opn*^{Hep} Tg mice developed spontaneous liver fibrosis over time in the absence of an exogenous profibrogenic stimuli [1], which was confirmed by western blot analysis for collagen-I protein (Supplementary Figure 3A). Thus, we asked whether overexpression of OPN in hepatocytes could also up-regulate HMGB1 expression and perhaps determine its cellular compartmentalization in these mice. We found significant increase in OPN

and HMGB1 expression as depicted by western blot, IHC and morphometry analysis (Supplementary Figure 3B-3C) along with a decrease in the ratio of nuclear-to-total and an increase in the ratio of cytoplasmic-to-total HMGB1 protein expression (Supplementary Figure 3D) in aging *Opn*^{Hep} Tg compared to WT mice.

SUPPLEMENTARY REFERENCES

- 1 Urtasun R, Lopategi A, George J, Leung TM, Lu Y, Wang X, *et al.* Osteopontin, an oxidant stress sensitive cytokine, up-regulates collagen-I via integrin alpha(V)beta(3) engagement and PI3K/pAkt/NFkappaB signaling. *Hepatology* 2012;**55**:594-608.
- 2 Wang X, Lopategi A, Ge X, Lu Y, Kitamura N, Urtasun R, *et al.* Osteopontin induces ductular reaction contributing to liver fibrosis. *Gut* 2014;**63**:1805-18.
- 3 Ge X, Antoine DJ, Lu Y, Arriazu E, Leung TM, Klepper AL, *et al.* High mobility group box-1 (HMGB1) participates in the pathogenesis of alcoholic liver disease (ALD). *The Journal of biological chemistry* 2014;**289**:22672-91.
- 4 Nieto N, Friedman SL, Cederbaum AI. Stimulation and proliferation of primary rat hepatic stellate cells by cytochrome P450 2E1-derived reactive oxygen species. *Hepatology* 2002;**35**:62-73.
- 5 Dignam JD, Lebovitz RM, Roeder RG. Accurate transcription initiation by RNA polymerase II in a soluble extract from isolated mammalian nuclei. *Nucleic acids research* 1983;**11**:1475-89.
- 6 Theise ND. Liver biopsy assessment in chronic viral hepatitis: a personal, practical approach. *Modern pathology : an official journal of the United States and Canadian Academy of Pathology, Inc* 2007;**20 Suppl 1**:S3-14.
- 7 Kleiner DE, Brunt EM, Van Natta M, Behling C, Contos MJ, Cummings OW, *et al.* Design and validation of a histological scoring system for nonalcoholic fatty liver disease. *Hepatology* 2005;**41**:1313-21.
- 8 Mormone E, Lu Y, Ge X, Fiel MI, Nieto N. Fibromodulin, an oxidative stress-sensitive proteoglycan, regulates the fibrogenic response to liver injury in mice. *Gastroenterology* 2012;**142**:612-21 e5.

- 9 Nieto N, Friedman SL, Cederbaum AI. Cytochrome P450 2E1-derived reactive oxygen species mediate paracrine stimulation of collagen I protein synthesis by hepatic stellate cells. *The Journal of biological chemistry* 2002;**277**:9853-64.
- 10 Antoine DJ, Williams DP, Kipar A, Jenkins RE, Regan SL, Sathish JG, *et al.* High-mobility group box-1 protein and keratin-18, circulating serum proteins informative of acetaminophen-induced necrosis and apoptosis in vivo. *Toxicological sciences : an official journal of the Society of Toxicology* 2009;**112**:521-31.
- 11 Antoine DJ, Jenkins RE, Dear JW, Williams DP, McGill MR, Sharpe MR, *et al.* Molecular forms of HMGB1 and keratin-18 as mechanistic biomarkers for mode of cell death and prognosis during clinical acetaminophen hepatotoxicity. *Journal of hepatology* 2012;**56**:1070-9.
- 12 Nystrom S, Antoine DJ, Lundback P, Lock JG, Nita AF, Hogstrand K, *et al.* TLR activation regulates damage-associated molecular pattern isoforms released during pyroptosis. *The EMBO journal* 2013;**32**:86-99.
- 13 Yang H, Lundback P, Ottosson L, Erlandsson-Harris H, Venereau E, Bianchi ME, *et al.* Redox modification of cysteine residues regulates the cytokine activity of high mobility group box-1 (HMGB1). *Molecular medicine* 2012;**18**:250-9.
- 14 Bonaldi T, Talamo F, Scaffidi P, Ferrera D, Porto A, Bachi A, *et al.* Monocytic cells hyperacetylate chromatin protein HMGB1 to redirect it towards secretion. *The EMBO journal* 2003;**22**:5551-60.
- 15 Skatchkov MP, Sperling D, Hink U, Mulsch A, Harrison DG, Sindermann I, *et al.* Validation of lucigenin as a chemiluminescent probe to monitor vascular superoxide as well as basal vascular nitric oxide production. *Biochemical and biophysical research communications* 1999;**254**:319-24.
- 16 Goodwin M, Herath C, Jia Z, Leung C, Coughlan MT, Forbes J, *et al.* Advanced glycation end products augment experimental hepatic fibrosis. *Journal of gastroenterology and hepatology* 2013;**28**:369-76.

- 17 Miura K, Yang L, van Rooijen N, Brenner DA, Ohnishi H, Seki E. Toll-like receptor 2 and palmitic acid cooperatively contribute to the development of nonalcoholic steatohepatitis through inflammasome activation in mice. *Hepatology* 2013;**57**:577-89.
- 18 Vespasiani-Gentilucci U, Carotti S, Perrone G, Mazzarelli C, Galati G, Onetti-Muda A, *et al.* Hepatic toll-like receptor 4 expression is associated with portal inflammation and fibrosis in patients with NAFLD. *Liver international : official journal of the International Association for the Study of the Liver* 2015;**35**:569-81.
- 19 Miura K, Kodama Y, Inokuchi S, Schnabl B, Aoyama T, Ohnishi H, *et al.* Toll-like receptor 9 promotes steatohepatitis by induction of interleukin-1beta in mice. *Gastroenterology* 2010;**139**:323-34 e7.

SUPPLEMENTARY TABLE

Supplementary Table 1. List of commercially available Abs used.

Target	Ab	Source
Acetylated Lysines	9441	Cell Signaling
Actin	sc-1616	Santa Cruz Biotechnology
Akt1/2/3	sc-1618	Santa Cruz Biotechnology
Calnexin	sc-6465	Santa Cruz Biotechnology
Collagen-I	MAB3391	Chemicon
Desmin	sc-23879	Santa Cruz Biotechnology
GAPDH	sc-20357	Santa Cruz Biotechnology
HDAC1	5356	Cell Signaling
HDAC2	5113	Cell Signaling
HDAC3	3949	Cell Signaling
HDAC4	7628	Cell Signaling
HDAC5	2082	Cell Signaling
HDAC6	7558	Cell Signaling
HMGB1 (IHC/ICC, IF)	ab18256	Abcam
HMGB1 (WB)	sc-56698	Santa Cruz Biotechnology
HNF4 α	sc-6556	Santa Cruz Biotechnology
Nucleoporin p62	610497	BD Biosciences
OPN	sc-21742	Santa Cruz Biotechnology
p300	ab3164	Abcam
p-Akt1/2/3	sc-7985-R	Santa Cruz Biotechnology
PCAF	3378	Cell Signaling
PI3K	sc-7189	Santa Cruz Biotechnology
RAGE	sc-5563	Santa Cruz Biotechnology
RAGE	AF1179	R&D Systems
β -Tubulin	T4026	Sigma

SUPPLEMENTARY FIGURES

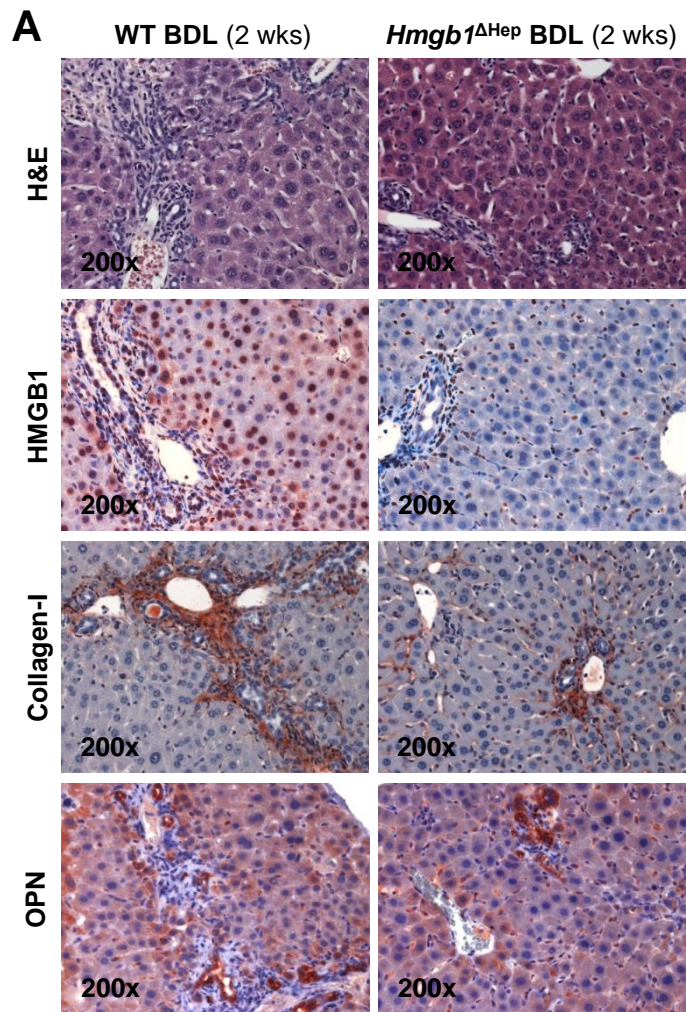
Supplementary Figure 1. *Hmgb1* ablation in hepatocytes partially prevents BDL-induced liver fibrosis in mice. *Hmgb1*^{ΔHep} and control littermates were bile duct ligated for 2 wks. H&E staining (**A, top**) and pathology scoring (**B**) show lower necrosis, inflammation, hepatocyte ballooning degeneration, fibrosis and ductular reaction in *Hmgb1*^{ΔHep} compared to control littermates. IHC shows reduced HMGB1 and collagen-I deposition in livers from BDL *Hmgb1*^{ΔHep} compared to control littermates (**A, middle**) whereas OPN expression remained similar (**A, bottom**). The results are expressed as fold-change of the MO-injected control littermates, which are assigned a value of 1 and are mean values ± SEM; *n*=8/group. •*p*<0.05, ••*p*<0.01 and •••*p*<0.001 for BDL *Hmgb1*^{ΔHep} vs. control littermates.

Supplementary Figure 2. rHMGB1 signals via RAGE to up-regulate collagen-I expression in HSCs. *Rage* or *Tlrs2/4/9* were ablated using siRNA. HSCs were treated with rHMGB1 and collagen-I expression was evaluated by western blot. The results are expressed as fold-change of the scrambled siRNA control, which is assigned a value of 1 and are mean values.

Supplementary Figure 3. Aging *Opn*^{Hep} Tg mice show elevated HMGB1 expression and develop spontaneous fibrosis. OPN, HMGB1 and collagen-I expression in livers from aging *Opn*^{Hep} Tg compared to WT mice. Western blot analysis for OPN, HMGB1 and collagen-I in total liver from 1 yr old WT and *Opn*^{Hep} Tg mice. The results are expressed as fold-change of the WT mice, which are assigned a value of 1. Results are mean values ± SEM. *n*=8/group. •••*p*<0.001 for *Opn*^{Hep} Tg vs. WT mice (**A**). IHC analysis of OPN (yellow arrows) and HMGB1 (green arrows) in liver from 1 yr old WT and *Opn*^{Hep} Tg mice (**B**). Total OPN and HMGB1 morphometry analysis (**C**) and quantification of total, nuclear and cytoplasmic as well as the ratios of nuclear-to-total and of cytoplasmic-to-total HMGB1 (**D**). The results from the morphometry analysis are

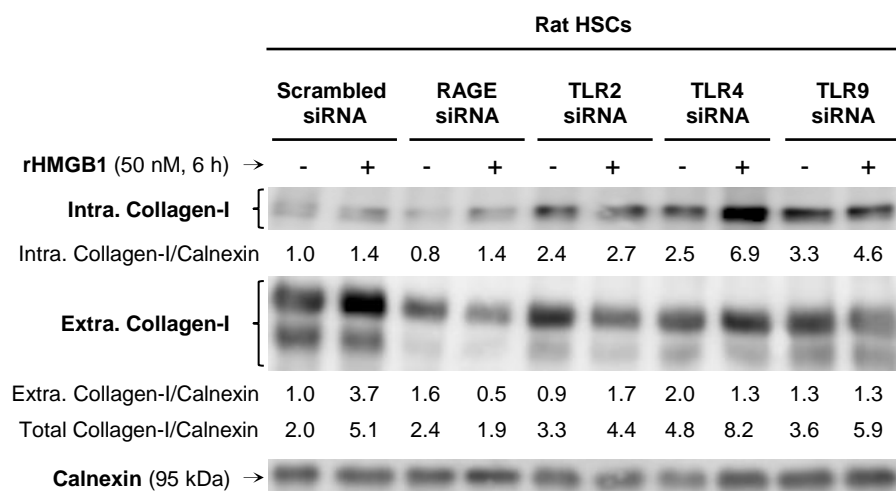
expressed as fold-change of the WT mice, which are assigned a value of 1 and are shown as mean values \pm SEM. n=8/group. $\bullet\bullet p<0.01$ and $\bullet\bullet\bullet p<0.001$ for *Opn*^{Hep} Tg vs. WT mice.

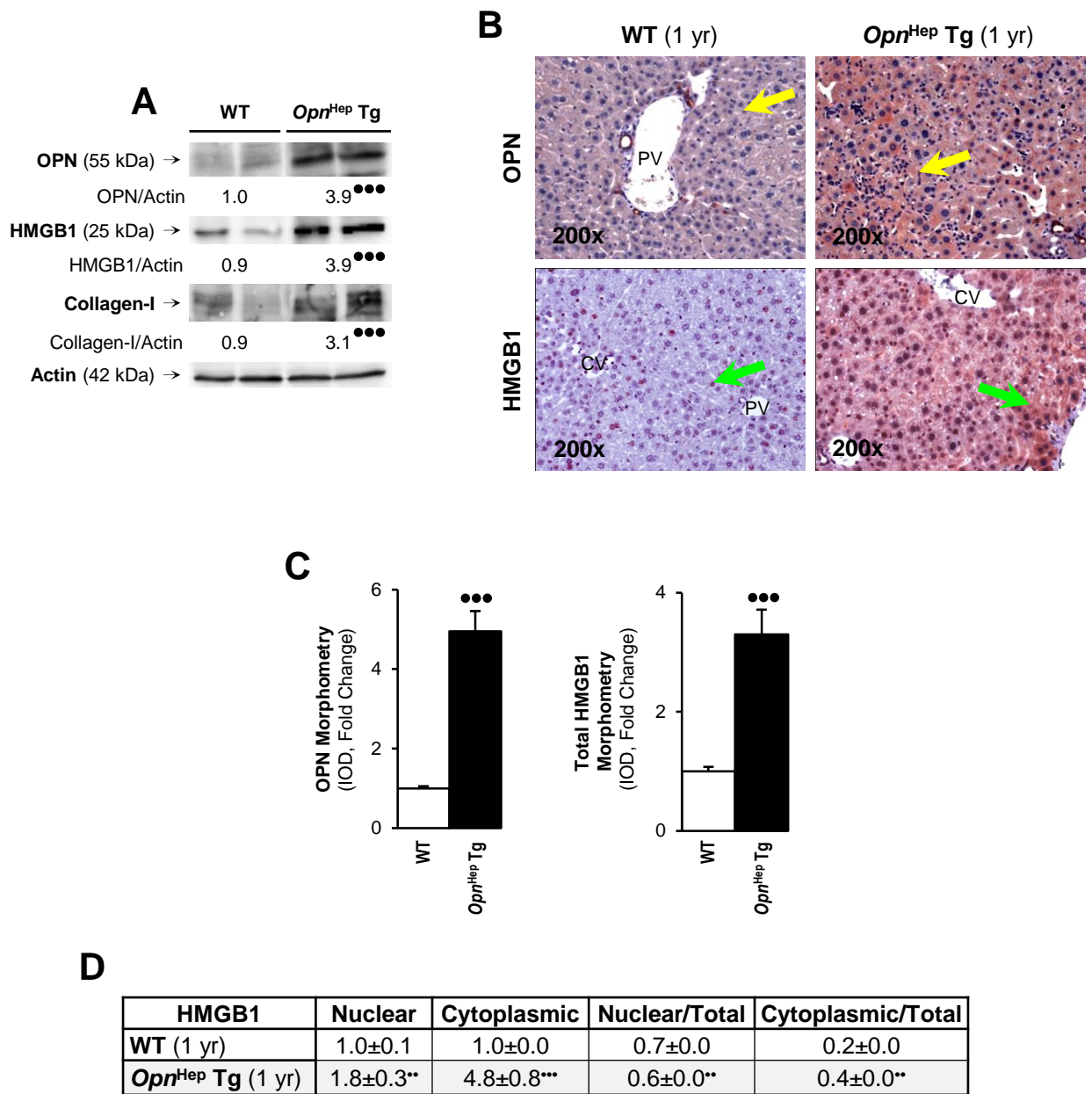
Supplementary Figure 4. Proposed mechanism. We previously demonstrated that chronic liver injury and reactive oxygen species induce OPN expression in hepatocytes, HSCs, biliary epithelial cells and oval cells. We showed that OPN engages $\alpha_v\beta_3$ integrin and signals via the PI3K-pAkt1/2/3-NF κ B pathway leading to up-regulation of intra- and extracellular collagen-I protein in HSCs (black and white-labeled pathway, *Hepatology* 2012;55(2):594-608). We also established that OPN reduces hepatocyte proliferation and activates the oval cell compartment giving rise to biliary epithelial cells. Furthermore, we identified that OPN increases and/or maintains TGF β expression in biliary epithelial cells, which along with OPN, signals to HSCs to increase their pro-fibrogenic potential (black and white-labeled pathway, *Gut* 2014;63(11):1805-18). In the present study, we demonstrate significant co-induction of OPN and HMGB1 following liver injury. Additionally, we show that OPN is upstream of HMGB1 in hepatocytes and HSCs. Our hypothesis was that OPN could participate in the pathogenesis of liver fibrosis by increasing HMGB1 to up-regulate collagen-I expression. We now show that well-established liver fibrosis along with marked induction of HMGB1 occurs in CCl₄-injected *Opn*^{Hep} Tg yet it is less in WT and almost absent in *Opn*^{-/-} mice. *Hmgb1* ablation in hepatocytes (*Hmgb1* ^{Δ Hep}) protects from CCl₄-induced liver fibrosis. Co-culture with hepatocytes that secrete OPN plus HMGB1 and challenge with either rOPN or rHMGB1 enhances collagen-I expression in HSCs, which is blunted by neutralizing Abs or by *Opn* and *Hmgb1* ablation. rOPN induces acetylation of HMGB1 in HSCs due to increased NADPH oxidase activity and the associated decrease in HDACs1/2 leading to up-regulation of collagen-I. Last, we demonstrate that rHMGB1 signals via RAGE activating the PI3K-pAkt1/2/3 pathway to up-regulate collagen-I (Please, see the strategies used to prove our hypothesis written in blue font).

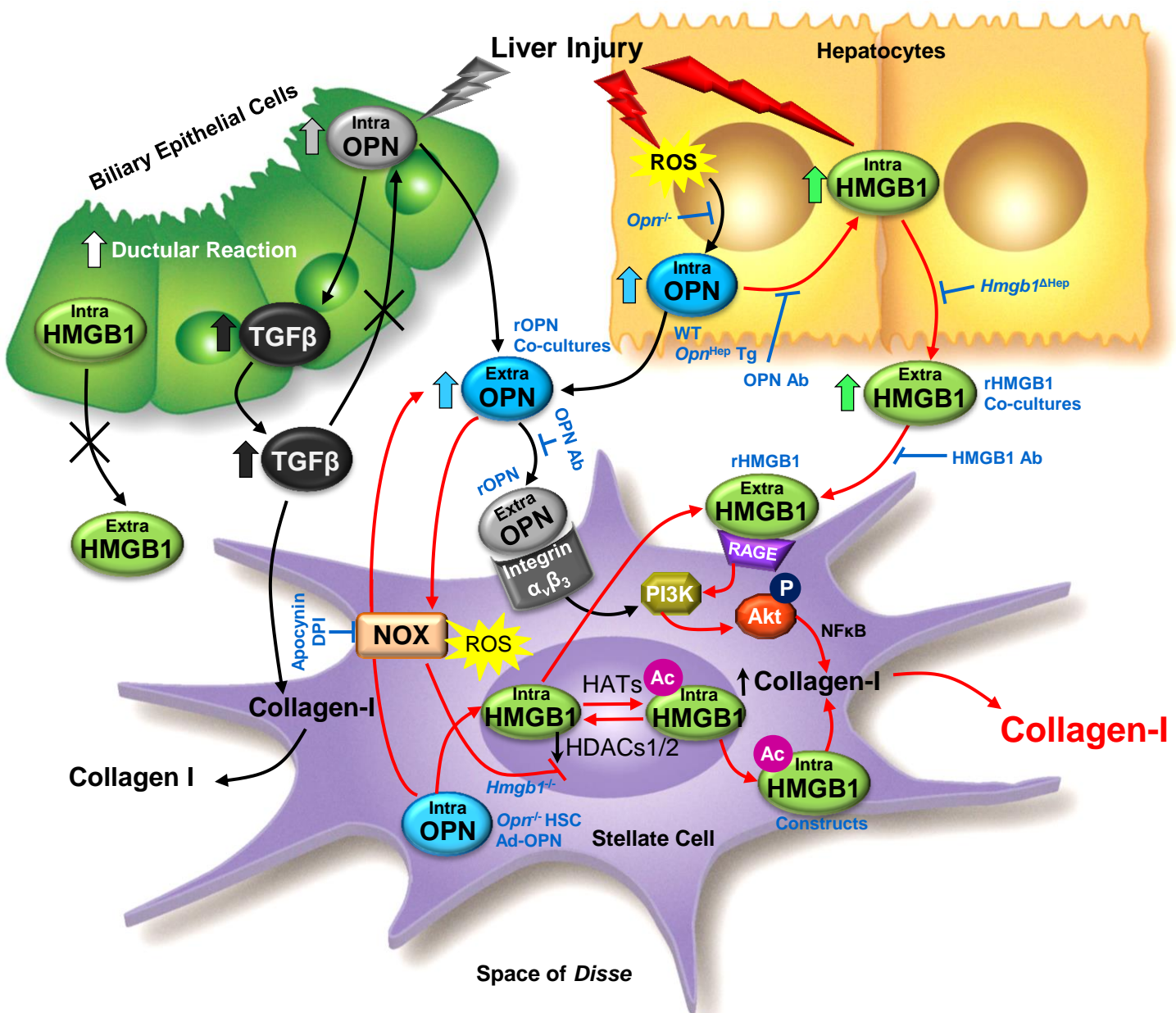


B

	Necrosis	Inflammation	Ballooning	Fibrosis	Ductular reaction
WT + BDL	0.79±0.18	1.86±0.07	0.43±0.02	2.96±0.12	3.42±0.36
<i>Hmgb1</i> ^{ΔHep} + BDL	0.47±0.11*	1.21±0.14*	0.25±0.06*	1.35±0.15**	1.26±0.14***







Supplementary Figure 4